TÉCNICO LISBOA

Searching for Beyond the Standard Model particles decaying to muon pairs with SND@LHC

Henrique de Sousa Santos

Thesis to obtain the Master of Science Degree in

Engineering Physics

Supervisors: Prof. Nuno Teotónio Viegas Guerreiro Leonardo
Dr. Cristóvão Vilela

Examination Committee

Chairperson: Prof. Mário João Martins Pimenta
Supervisors: Prof. Nuno Teotónio Viegas Guerreiro Leonardo
Members of the Committee: Dr. Catarina Quintans
Dr. Simona Ilieva

October 2024

Declaration

I declare that this document is an original work of my own authorship and that it fulfills all the requirements of the Code of Conduct and Good Practices of the Universidade de Lisboa.

Acknowledgments

I would like to thank my family for always allowing me to continue choosing my own path throughout my academic journey and for all the support and interest they have shown for my passions and endeavors. Through the easy times, the hard trials, the stressful deadlines, the celebrations of triumph, I always knew they would be in my corner every step of the way, and I am forever thankful.

To my friends and colleagues, without whom I could've never finished this journey. Even after I changed degrees, as our schedules drifted apart, and as quarantine made it all but easy to isolate ourselves, thank you for never letting me go and making me feel happy and like I belonged. I could not have done this without you. On the other hand, I thank my new friends and colleagues for the warm welcome and experiences throughout these last few years at MEFT.

To my supervisors Cristovão and Nuno, for all the guidance provided and for your eagerness to help me every step of the way as I tackled this thesis, with endless patience and availability. I would also like to thank FCT, LIP and particularly the SHiP and SND departments, for allowing me to receive a research grant and providing me with the opportunity to work alongside them and grow as a professional. —-

Resumo

Apesar do Modelo Padrão (SM) ser uma teoria muito bem sucedida, não é suficiente para explicar todos os problemas da física moderna. Torna-se assim necessário estender o SM utilizando física para além do Modelo Padrão (BSM). O Scattering and Neutrino Detector at the Large Hadron Collider (SND@LHC) é uma experiência compacta e autónoma cujo objetivo principal é a observação de neutrinos de colisionador. Nesta tese, realizamos o primeiro estudo de Partículas de Interação Débil (FIPs) em SND@LHC.

Esta análise foca-se mais na assinatura experimental de decaimento para dimuão do que na partícula que decai. O modelo de referência escolhido foi o Dark Higgs (DH), um escalar cuja interação com as partículas do SM decorre da mistura com o bosão de Higgs do SM. Esta FIP foi simulada utilizando o gerador Forward Experiment Sensitivity Estimator (FORESEE), com uma massa de $251.2MeV$ a decair no alvo do detetor. Com recurso a amostras de simulação de Monte-Carlo do ruído e de dados experimentais, foram implementados vários cortes de seleção, resultando num ruído de neutrinos de < 0.2 eventos e numa estimativa de ruído de muões na zona de sinal de 0.43 ± 0.43 em $200fb^{-1}$, correspondendo a 7 eventos necessários para a rejeição da hipótese de apenas ruído a 5σ e retendo 12.78% de eficiência de seleção do sinal. Podemos então esperar rejeição da hipótese de apenas ruído após, em média, 54 decaimentos de DH na região do alvo do detetor. Foram também excluídos ângulos de mistura de DH superiores a 10^{-3} para a massa estudada.

Palavras Chave

Scattering and Neutrino Detector, Partículas de Interação Débil, Dark Higgs, Procuras signature-driven, Eficiências de seleção, Rejeição de ruído

Abstract

Although the Standard Model (SM) is a very successful theory, it is not able to explain some of the outstanding problems of modern physics. For addressing these shortcomings, an extension of the SM using Beyond the Standard Model (BSM) physics is required.

The Scattering and Neutrino Detector at the Large Hadron Collider (SND@LHC) is a compact and stand-alone experiment recently installed at the LHC designed for the observation and measurement of collider neutrinos. In this thesis, we conduct the first search for Feebly Interacting Particle (FIP) at SND@LHC.

This analysis is signature driven, focusing on generic FIP decays to dimuons more than the specific nature of the decaying particle. As our benchmark model, we chose the Dark Higgs, a scalar which interacts with SM particles through mixing with the SM Higgs. This FIP was simulated using the Forward Experiment Sensitivity Estimator (FORESEE) tool with a mass of $251.2MeV$ and decay vertex in the detector target. Through the use of both Monte-Carlo background samples and collision data samples, several signal selection criteria were devised, culminating in an expected neutrino background of < 0.2 events and a muon background estimation in the signal region of 0.43 ± 0.43 over $200fb^{-1}$, corresponding to a 7 event background-only exclusion at 5σ. Simultaneously, this selection retains 13% of signal selection efficiency. Combining these values, we could expect background-only exclusion from, on average, 54 Dark Higgs decays on the target subsystem. Additionally, DH mixing angles above 10^{-3} are expected to be excluded for DH in our mass range.

Keywords

Scattering and Neutrino Detector, Feebly Interacting Particles, Dark Higgs, Signature-driven searches, Selection Efficiencies, Background Rejection

Contents

List of Figures

List of Tables

Acronyms

ATLAS A Toroidal LHC ApparatuS: LHC experiment

BAU Baryon Assymetry of the Universe

BSM Beyond the Standard Model

CL Confidence Level

CMS Compact Muon Solenoid: LHC experiment

DH Dark Higgs: Feebly Interacting Particle

DS Downstream: System of the SND@LHC detector

ET Emulsion Target: System of the SND@LHC detector

FASER ForwArd Search ExpeRiment

FCC Future Circular Collider

FIP Feebly Interacting Particle

FORESEE FORward Experiment SEnsitivity Estimator

HC Hadronic Calorimeter

IP Interaction Point

LHC Large Hadron Collider

MC Monte Carlo (simulation)

MS Muon System

QDC Charge-to-Digital Converter

SciFi Scintillating Fiber

SiPM Sillicon PhotoMultipliers

SM Standard Model

SND@LHC Scattering and Neutrino Detector at the Large Hadron Collider

SPS Super Proton Synchrotron: CERN accelerator

SSB Spontaneous Symmetry Breaking

US Upstream: System of the SND@LHC detector

VEV Vacuum Expectation Value

VS Veto System: System of the SND@LHC detector

1

Introduction

Contents

The understanding of matter and its fundamental constituents has been a major issue for humanity since ancient times. Fast-forwarding from Plato's theory of the elements to the 20th century, particle physics began gaining more and more relevance as its own new branch of physics, focusing on the basic building blocks of matter. Finally in the late 1970s, to the credit of countless physicists and researchers, a theory to explain 3 of the 4 fundamental forces was formalized: The Standard Model [6].

The Standard Model (SM) accurately predicts most experimental results. However, the existence of dark matter and the lack of a good particle candidate for it, the fact that neutrinos are not massless and can oscillate between flavors and the baryon asymmetry of the universe (BAU) are just some of the questions that the SM cannot hope to answer without introducing new particles and formalisms to the theory. Searching for these answers is the role of Beyond the Standard Model (BSM) physics.

The search for BSM particles can be done in two complementary ways: probing the energy frontier and the intensity frontier, as illustrated in Figure 1.1. The focus is usually on the energy frontier, which focuses on the search of high-mass BSM particles. The path of exploring this frontier involves increasing the precision of SM process measurements and as such better the indirect study of such particles. This frontier can also be probed through an increase of the center of mass energy of the collisions ($\sqrt{s}$), which is dependent on improving the accelerators. The Future Circular Collider (FCC) [7] is one of the projects aligned with this philosophy.

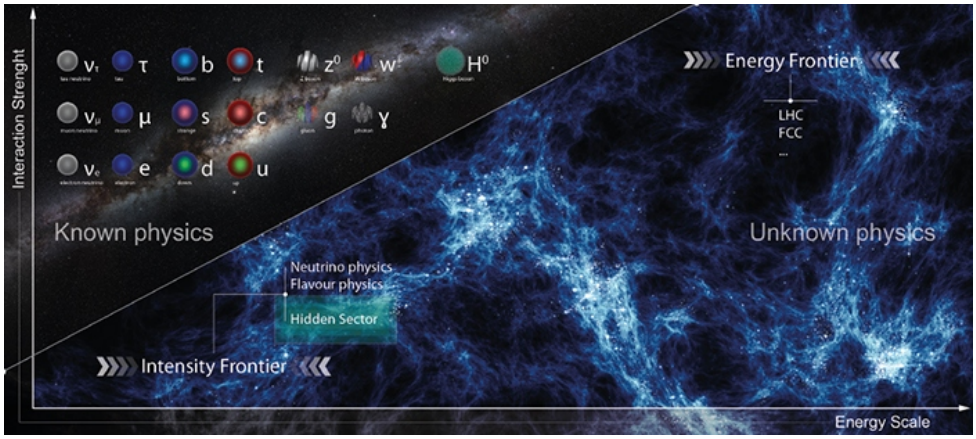

Figure 1.1: Frontiers of BSM searches. This image shows the known SM physics as just a corner of a much larger physics framework. The two axes off Interaction Strength and Energy Scale hint at the possible ways to expand our current physics knowledge. From [1].

However, this is not the only possibility. What if the reason why BSM particles have not yet been detected is not because they are heavy but because they interact feebly? This is the philosophy behind the study of the intensity frontier of particle physics, whose focus is on increasing the luminosity and precision of experiments in order to possibly detect such feebly interacting particles (FIPs).

1.1 Motivating a FIP study at SND@LHC

Just like FIP searches in the energy frontier have tough barriers to overcome, like achieving a high enough center of mass energy, so too is the case for searches in the intensity frontier. Many constraints present themselves as one probes the intensity frontier such as the need for detection methods that are sensitive to the rare interactions or decays of these particles. Additionally, the experimental setups must be capable of operating at high luminosity to increase the probability of interaction events, which often leads to challenges in managing the very large experimental background to be expected in this kind of studies.

The LHC provides the necessary conditions to study both BSM frontiers. The intensity frontier in particular will gather even more interest as LHC is soon entering the HL-LHC (High Luminosity LHC) phase.

CERN has no shortage of collaborations that study this facet of particle physics, and each provides a different but meaningful way to explore BSM physics. The SHiP experiment, a large fixed target experiment whose goal is to study the decay of FIPs originating from a high-intensity proton beam from the Super Proton Synchrotron (SPS), is one such collaboration, whose project has recently been approved for construction [8]. The Mathusla collaboration, on the other hand, proposes a large-scale, relatively simple detector located at surface level to search for long lived particles (LLP) produced in LHC proton-proton collisions, with the added bonus of being able to act as a cosmic ray telescope. The NA62 experiment, which has been taking data since 2015, is another fixed-target experiment at the SPS. Designed for studying rare kaon decays through the collision of high-energy protons with a beryllium target, it can also partake in BSM studies, particularly in the search for LLPs.

Focusing on the forward region (low angles with the beam axis, high pseudorapidity) of the ATLAS interaction point, we can encounter the sister experiments: Scattering and Neutrino Detector at the LHC (SND@LHC) and ForwArd Search ExpeRiment at the LHC (FASER). Although the two experiments have the similar purpose of detecting neutrinos and searching for FIPs, they explore different pseudo-rapidity ranges and their detectors are quite different.

FASER [9] focuses on neutrinos with pseudo-rapidity $\eta > 9$. Like SND@LHC, it features an emulsion vertex detector, which it complements with a spectrometer. The Scattering and Neutrino Detector at the Large Hadron Collider (SND@LHC) [4] is a compact stand-alone experiment that began operation in 2022, at the beginning of the LHC Run3. The experiment was built in the previously unused TI18 tunnel, 480 meters away from the ATLAS interaction point (IP), in the forward region, and was designed to perform high energy neutrino measurements in the pseudo-rapidity region $7.2 < \eta < 8.4$. Like FASER, the experiment makes use of nuclear emulsion and electronic detector technologies, acting together to guarantee better resolution and sensitivity.

A detailed description of the detector is given in chapter 3, but it is already clear that some of the

features of the SND@LHC experiment are equally as advantageous to FIP studies as to neutrino studies. Firstly, the location of the experiment in the far-forward region gives SND@LHC and FASER two major advantages when it comes to FIP studies: proton collisions produce many hadrons in the forward region, which can then decay to both neutrinos and FIPs. Hence, the near collinearity with the beam guarantees a high flux of the types of particles we aim to study, a very important part on any BSM studies in the intensity frontier. On the other hand, being 480 meters away from the IP, including 100 meters of solid rock, paired with dipole magnets that stear charged particles away from collinearity, helps tremendously in reducing the experimental background. Even if other experiments like ATLAS and CMS had instrumentation in the same forward direction, they would be less sensitive to FIP events due to the the massive background caused by other particles.

One can also compare the viability of FIP studies at SND with similar studies for fixed-target experiments, such as NA62 and SHiP. In that case, the advantages of conducting the study on the SND@LHC experiment centers around the higher energy of collisions: higher collision energy allows for the production of heavier hadrons, which can in turn decay to heavier FIPs.

1.2 Objectives and thesis organization

This thesis aims to conduct the first FIP analysis study at SND@LHC. This analysis is signature driven, as we are more concerned with the experimental signature of the studied decay mode than the specific nature of the decaying particle. As will be apparent after the detector description in chapter 3, the SND@LHC's electronic detectors are particularly sensitive to FIP decays to muon pairs. Dimuons, like single muons, form a robust experimental signature, hence why this decay mode was chosen for the project. This project's goal is to achieve an estimate of the number of FIP to dimuon decay events that would result in a 5σ experimental observation or a 90% confidence level (CL) exclusion. An important detail of this project is that all the methods developed to achieve these results aim to be model-independent, with the Dark Higgs (DH) being used as a benchmark particle while conducting the study. More details about this feebly interacting particle will be discussed in chapter 2.

The thesis is divided into 7 chapters: 1-Introduction;2- From the Standard Model to FIPs; 3-The Scattering and Neutrino Detector experiment; 4-Signal and Background models; 5- Event Selection and Reconstruction;6-Likelihood Threshold Optimization and Background Estimation;7- Closing remarks.

2

From the Standard Model to FIPs

Contents

2.1 The Standard Model of Particle Physics

The Standard Model of particle physics is arguably the greatest accomplishment in all scientific progress of the 20th century. It describes the fundamental particles, their interactions and explains 3 of the 4 fundamental forces: the electromagnetic force, weak nuclear force and strong nuclear force, leaving out only gravity. The Standard Model is also one of the most successful theories ever in terms of its predictive power: the vast majority of experimental observables agree with the correspondent SM predictions with incredible precision and after 2012, with the experimental discovery of the Higgs boson by both the CMS [10] and ATLAS [11] collaborations, all the particles it proposes have been found. It has been the result of numerous contributions from physicists over decades: the theoretical groundwork on the gauge theory by Yang and Mills in 1954 [12], followed by Glashow's electroweak theory in 1961 [13], Weinberg and Salam's addition of the Higgs mechanism in 1967 [14], Hooft and Veltman's proof of renormalizability of the SM [15] and many others.

The Standard Model is built upon the concept of gauge invariance, leading to the description of fundamental forces through gauge bosons. In particular, the SM Lagrangian is both globally and locally invariant under the gauge group

$$U(1)_Y \times SU(2)_L \times SU(3)_c \tag{2.1}$$

where Y is the conserved $U(1)$ hypercharge, L is the left-handed weak isospin (the invariants of the electroweak theory) and c is the color charge, conserved in the strong interaction. The $U(1)$ gauge group gives us one gauge boson, and each SU(N) group gives us N^2-1 gauge bosons (3 and 8 for SU(2) and SU(3) respectively). These are the eight gluons in the case of SU(3) (G^a_μ). For the electroweak theory, the 4 physical particle bosons (photon, W^+,W^- and Z) come from a mixing of the 4 electroweak gauge fields: the U(1)'s B_μ and the SU(2)'s three W^i_μ.

For the fermions, as long as they transform under the symmetries of the gauge group in equation 2.1, there are no symmetry constraints imposed by the SM on the number of fermions. Experimentally, physicists have discovered 3 generations of SU(2) doublets for both quarks and leptons. Additionally, some experimental measurements on the Z-boson decay suggest that, at least for the number of light neutrinos, 3 is all there is to find [16].

The final major piece of the Standard Model is the Higgs mechanism, based on spontaneous symmetry breaking (SSB), responsible for the masses of both fermions and bosons. Due to its parallel with our benchmark FIP, this mechanism warrants further detail, which we will expand upon in subsection 2.1.1.

All SM fields and relevant charges are presented in Table 2.1. Now we can write the Standard Model Lagrangian, where the terms are locally invariant under the SM gauge. The Lagrangian can be simplified

into:

$$\mathcal{L} = -\frac{1}{4}F_{\mu\nu}F^{\mu\nu} + \left(i\overline{\Psi}\not{D}\Psi + h.c.\right) + \left(y_{ij}\overline{\Psi}_i\Psi_j\Phi + h.c\right) + \left|D_\mu\Phi\right|^2 - V\left(\Phi\right) + \mathcal{L}_{\mathcal{QCD}}. \tag{2.2}$$

where each term actually represents multiple similar terms. We will focus on the electroweak part of the Lagrangian, condensing the QCD terms in $\mathcal{L}_{\mathcal{QCD}}$.

$-\frac{1}{4}F_{\mu\nu}F^{\mu\nu}$ represents the gauge field kinetic terms, where $F^{\mu\nu}$ is the field strength tensor for a given gauge field. For a generic gauge field A:

$$F_{\mu\nu} = \partial_\mu A_\nu - \partial_\nu A_\mu + ig\left[A_\mu, A_\nu\right] \tag{2.3}$$

where g is that specific gauge's coupling constant and the square bracket term is a commutator, which is generally non-zero. The term $\left(i\overline{\Psi}\not{D}\Psi + h.c.\right)$ condenses both the kinetic terms and gauge interactions terms of fermion fields. Here, Ψ represent a fermion field ($\overline{\Psi}$ is the Dirac adjoint), and $\not{D} = \gamma^\mu D_\mu$, with the covariant derivative:

$$D_\mu = \partial_\mu - ig_w W_\mu^a T^a - ig_Y Y B_\mu \tag{2.4}$$

We will leave the terms related to the Higgs for subsection 2.1.1.

Gauge Fields				
$\mathbf{U(1)_Y}$	B_μ			
$\mathbf{SU(2)_L}$	$W_\mu^i, i = 1,2,3$			
$\mathbf{SU(3)_c}$	$G_\mu^a, a = 1,...,8$			
Higgs Doublet		Y	T_3	Q
	$\phi = \begin{pmatrix}\phi^+\\ \phi^0\end{pmatrix}$	1 1	$\frac{1}{2}$ $-\frac{1}{2}$	1 0
Fermion Fields		Y	T_3	Q
Leptons	$\begin{pmatrix}\nu_{e_{iL}}\\ e_{iL}\end{pmatrix} = \left\{\begin{pmatrix}\nu_{e_L}\\ e_L\end{pmatrix}; \begin{pmatrix}\nu_{\mu_L}\\ \mu_L\end{pmatrix}; \begin{pmatrix}\nu_{\tau_L}\\ \tau_L\end{pmatrix}\right\}$ $e_{iR} = \{e_R, \mu_R, \tau_R\}$	-1 -1 -2	$\frac{1}{2}$ $-\frac{1}{2}$ 0	0 -1 -1
Quarks	$\begin{pmatrix}u_{iL}\\ d_{il}\end{pmatrix} = \left\{\begin{pmatrix}u_L\\ d_L\end{pmatrix}; \begin{pmatrix}c_L\\ s_L\end{pmatrix}; \begin{pmatrix}t_L\\ b_L\end{pmatrix}\right\}$ $u_{iR} = \{u_R, c_R, t_R\}$ $d_{iR} = \{d_R, s_R, b_R\}$	$\frac{1}{6}$ $\frac{1}{6}$ $\frac{4}{3}$ $-\frac{2}{3}$	$\frac{1}{2}$ $-\frac{1}{2}$ 0 0	$\frac{2}{3}$ $-\frac{1}{3}$ $\frac{2}{3}$ $-\frac{1}{3}$

Table 2.1: Fields of the Standard Model: Y, T_3 and Q are, respectively, the hypercharge, third component of weak isospin and electromagnetic charge of the field. The Higgs doublet has spin 0, so chirality (left or right handedness) does not apply.

2.1.1 The Higgs mechanism

The Higgs mechanism assumes the existence of a weak isospin doublet of fields. Consider also the Lagrangian of this doublet:

$$\phi = \begin{pmatrix} \phi^+ \\ \phi^0 \end{pmatrix} \qquad \mathcal{L} = (\partial_\nu \phi)^\dagger (\partial^\nu \phi) - V(\phi) = (\partial_\nu \phi)^\dagger (\partial^\nu \phi) - \mu^2 \phi^\dagger \phi - \lambda (\phi^\dagger \phi)^2 \tag{2.5}$$

By selecting appropriate limits for our potential's parameters ($\mu^2 < 0$ and $\lambda > 0$), we arrive at an infinite ring of degenerate minima, obtained from:

$$\phi^2 = -\frac{\mu^2}{2\lambda} \tag{2.6}$$

However, there can only be a single physical vacuum state, which we can pick without loss of generality to be:

$$\langle 0|\phi|0\rangle = \frac{1}{\sqrt{2}} \begin{pmatrix} 0 \\ v \end{pmatrix} \tag{2.7}$$

By expanding around the chosen VEV as:

$$\Phi = \begin{pmatrix} \phi^+ \\ v + \frac{H + i\xi}{\sqrt{2}} \end{pmatrix} \tag{2.8}$$

We can now expand the Higgs Lagrangian from equation 2.5 (which can be made gauge invariant by substituting the covariant derivative from equation 2.4 in place of the partial derivatives). From this arise terms involving the Higgs and its interactions with boson fields, as well as some terms involving three pseudo-Goldstone bosons associated with the broken symmetries. These Goldstone bosons are absorbed by three electroweak gauge bosons (W^+,W^- and Z), providing them with their longitudinal components and thereby giving them mass.

This explains the $|D_\mu \Phi|^2 - V(\Phi)$ terms in equation 2.2: they describe the interaction of the Higgs boson with itself and with the gauge bosons. The final term contains the interaction of the Higgs boson with the fermions, granting them mass. Here, y_{ij} are known as the Yukawa couplings, which dictate the strength of each particle's interaction with the Higgs.

The terms in the SM Lagrangian are not enough to solve all of the problems in modern particle physics, leaving us the door open for BSM physics and the existence of FIPs. Although this project aims for model independence, let us now focus on our benchmark scenario.

2.2 Feebly Interacting Particles

In the search for physics beyond the Standard Model, various theoretical frameworks propose different "portals" through which new particles and interactions can communicate with the known particles of the Standard Model. These portals are categorized based on the types of new particles introduced and their interactions with Standard Model fields [17].

When adding BSM particles to the Standard Model, one must delve into the formalism of portals [18] [19]. The portal framework is a generic setup for combining an operator composed from SM fields and one composed from BSM fields using an interaction Lagrangian. The simplest renormalizable portals, with the lowest dimensions, can be separated into four different types:

- Vector Portals, like the Dark Photon.
- Scalar Portals, like the Dark Higgs.
- Fermion Portals, like Sterile Neutrinos.
- Pseudo-scalar Portals, like Axions.

The vector portal allows the dark photon to interact with Standard Model particles through kinetic mixing with the photon or the Z boson. It is a very common portal due to emerging very naturally in various theoretical frameworks, such as hidden U(1) gauge extensions. The pseudo-scalar portal, on the other hand, involves adding axions or axion-like particles (ALPs). This portal is particularly attractive when studying the strong CP problem or spontaneously broken global symmetries. The fermion portal, by introducing new fermionic degrees of freedom, could solve problems such as explaining neutrino masses and baryogenesis.

This thesis will focus on the scalar portal, using the Dark Higgs as its benchmark particle.

2.2.1 The Dark Higgs

With the discovery of the Higgs boson, the search for more scalar and pseudo-scalar particles is pursued. These potential scalar particles would interact with the SM through mixing with the SM-Higgs boson. This portal is also particularly attractive due to its minimal assumptions, minimal changes to the SM, and potential for direct detection through Higgs-related processes. The Dark Higgs model that is considered in this thesis [2] consists in adding a new real scalar field h' to the Higgs potential, such that the BSM portal would be the quartic scalar interaction. The new potential containing this DH can be written as:

$$V_H = \mu_H^2|H|^2 - \frac{1}{4}\lambda_H|H|^4 + \mu'^2 h'^2 - \mu'_3 h'^3 - \frac{1}{4}\lambda' h'^4 - \mu'_{12} h'|H|^2 - \epsilon h'^2|H|^2$$

where H is the SM Higgs doublet and all the couplings have the appropriate energy units, with the last term being the aforementioned quartic scalar interaction. To find the physical particles, like was done with the Higgs in the SM, one must minimize the potential, choose a single physical minimum and diagonalize the mass terms. The resultant particles are the SM-like Higgs h and the dark Higgs boson ϕ.

This new interaction, after applying some constraints related to the SM-Higgs parameters like its mass and VEV (125 GeV and 246 GeV), contains five free parameters. It is beneficial to reduce the degrees of freedom of a theory to increase its predictive power. To accomplish this, one can add extra constraints to the potential couplings, like enforcing relations between the couplings (like $\mu_3' = \mu_{12}'$) or setting couplings to zero.

For the purposes of this thesis, we will be using a phenomenological parametrization [2], such that the Lagrangian for the Dark Higgs boson ϕ is:

$$\mathcal{L} = -\frac{1}{2}m_\phi^2\phi^2 - \sin\theta\frac{m_f}{v}\overline{f}f - \lambda v h\phi\phi + ... \tag{2.9}$$

where f is any massive fermion, m_ϕ, θ and λ are the dark Higgs boson mass, mixing angle and trilinear coupling and we are omitting terms with cubic and quartic scalar interaction between our scalar particles. The mixing angle quantifies the interaction between the Dark Higgs and the SM Higgs.

2.2.2 Dark Higgs Production

For this thesis, we will be focusing on production modes from meson decays, since, for currently viable values of DH parameters, these have been shown to be the main contributors to Dark Higgs rates in forward-region experiments [2]. The following diagrams were designed based on the production methods described in [2] which are, from most to least dominant:

1. B meson decay

   The dark Higgs inherits couplings from the SM Higgs, which causes it to be preferentially involved in processes involving heavy flavours. Of these, the decay of B mesons has been shown to be the largest contributor to DH production.

   This decay ($B \to X_s\phi$, where X_s is any strange hadronic state) is dominated by the parton-level process $b \to s\phi$. This process does not happen at tree-level, and involves a $(u, c, t) - W$ loop, dominated by the top contribution, with the top quark radiating a ϕ, analogous to the SM-Higgs equivalent.

Uncertainties from strong interaction effects are minimized in the ratio:

$$\frac{\Gamma\left(B \to X_s \phi\right)}{\Gamma\left(B \to X_c e \nu\right)} = \frac{\Gamma\left(b \to s \phi\right)}{\Gamma\left(b \to c e \nu\right)} = \frac{27}{64\pi^2 v^2} \frac{m_t^4}{m_b^2} \left(1 - \frac{m_\phi^2}{m_b^2}\right)^2 \frac{1}{f_{c/b}} \left|\frac{V_{ts}^* V_{tb}}{V_{cb}}\right|^2 \theta^2 \tag{2.10}$$

where the V's are CKM matrix elements [20] and $f_{c/b} \simeq 0.51$ is the phase space factor for $b \to c e \nu$ [21].

Given the known value $B\left(B \to X_c e \nu\right) = 0.104$ for both B^0 and $B^\pm$ and since total width is θ-independent for $\theta \ll 1$, we can write:

$$B\left(B \to X_s \phi\right) \simeq 5.7 \left(1 - \frac{m_\phi^2}{m_b^2}\right)^2 \theta^2 \tag{2.11}$$

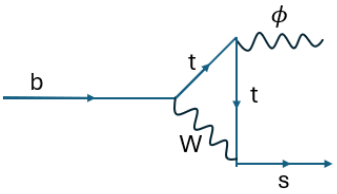

Figure 2.1: Diagram of the parton-level process $b \to s\, \phi$ involved in the production of Dark Higgs (ϕ) via B-meson decay.

2. K and light meson decays

   A dark Higgs can also be produced by the decay of K mesons, with the other product being a light meson. This decay once again involves $(u, c, t) - W$ loop dominated by the top quark contribution (figure 2.2). A smaller contribution to DH production can be attributed to light meson decays, such as $\eta' \to \eta\phi$, $\eta \to \pi^0 \phi$ and $\pi^\pm \to e\nu\phi$.

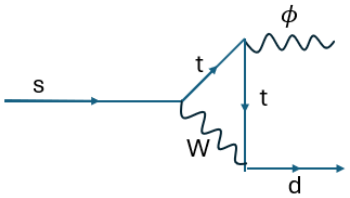

Figure 2.2: Diagram of the parton-level process $s \to d\, \phi$ involved in the production of Dark Higgs (ϕ) via K-meson decay.

As expected from DH's similarities to the SM Higgs, the hierarchy of branching fractions follows $B(B \to \phi) \gg B(K \to \phi) \gg B(\eta, \pi \to \phi)$.

2.2.3 Dark Higgs Decays

Focusing on the Dark Higgs' decay modes to SM-particles, there are various DH mass thresholds that govern which decays are possible, which will be taken into consideration when choosing the simulated mass of our FIP.

For a Dark Higgs mass $m_\phi < 2\ m_\pi$, the Dark Higgs has 2 modes it primarily decays to: electron-positron pairs (e^+e^-) and dimuon ($\mu^+\mu^-$), with decay widths of

$$\Gamma(\phi \longrightarrow \ell\ell) = \frac{m_\ell^2 m_\phi}{8\pi v^2}\left(1 - \frac{4m_\ell^2}{m_\phi^2}\right)^{\frac{3}{2}}\theta^2 \tag{2.12}$$

where $\ell = e, \mu$. Surpassing mass thresholds like $m_\phi > 2m_\pi$,$m_\phi > 2m_\tau$ or $m_\phi > 2m_K$ make possible other decay modes. Resonances and the decay to mesons are two of the main factors that complicate decay widths for higher mass ranges. Fortunately, as will be discussed after presenting the experiment, we wish to focus on decays to muon pairs, so there will be no need to venture into disputed territory for the decay widths. The branching fractions as a function of m_ϕ are represented in Figure 2.3

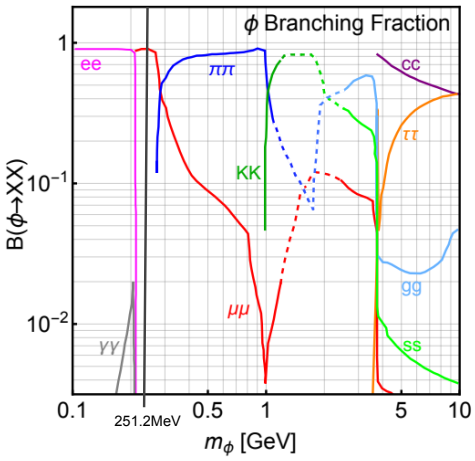

Figure 2.3: Dark Higgs branching fractions to SM particles as a function of m_ϕ. The selected mass for this project's FIP ($251.2MeV$) is represented by a vertical black line. From [2].

3

The Scattering and Neutrino Detector experiment

Contents

The Scattering and Neutrino Detector at the LHC is the latest built experiment at the LHC. It is a compact and stand-alone experiment designed for the observation of collider neutrinos. For an experiment like SND@LHC to be successful, there is a need for a high energy neutrino flux while keeping the background events low enough not to drown out any potential neutrino events. Since most experiments, like ATLAS and CMS, are located near the interaction point (IP) of the collisions, any neutrino data would be drowned by the enormous amount of background. This is why SND@LHC is such a privileged situation regarding collider neutrino detection: a lot of thought was put into not only massively reducing the background, but also easily identifying any background that might still remain, as will be seen in the following sections.

The SND@LHC detector is located 480m downstream of IP1, where the ATLAS detector is, in the previously unused TI18 tunnel. The detector is approximately collinear to the beam direction, with a slight offset. From all particles originally emitted in this axis towards the SND@LHC detector, very few actually reach the detector: the charged particles are steered away from their straight line path by the LHC magnets, and most neutral particles that remain will be stopped by the 100 meters of natural underground material between the LHC and TI18 tunnels along the beam direction. This severely reduces the background and allows for a proper study of collider neutrinos. The location schematic is shown in Figures 3.1 and 3.2. Furthermore, the offset that makes the detector only approximately collinear is shown in Figure 3.4.

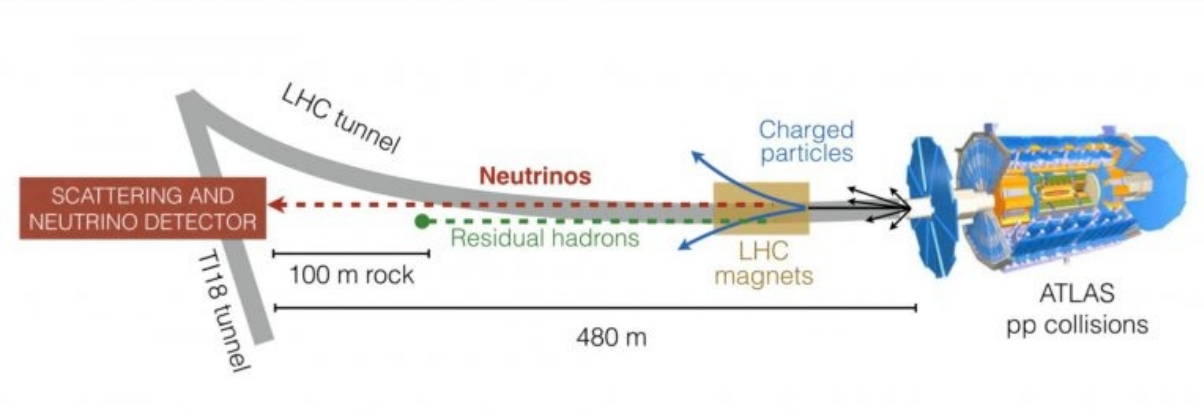

Figure 3.1: Location of the SND@LHC apparatus in relation to the ATLAS IP. From [3].

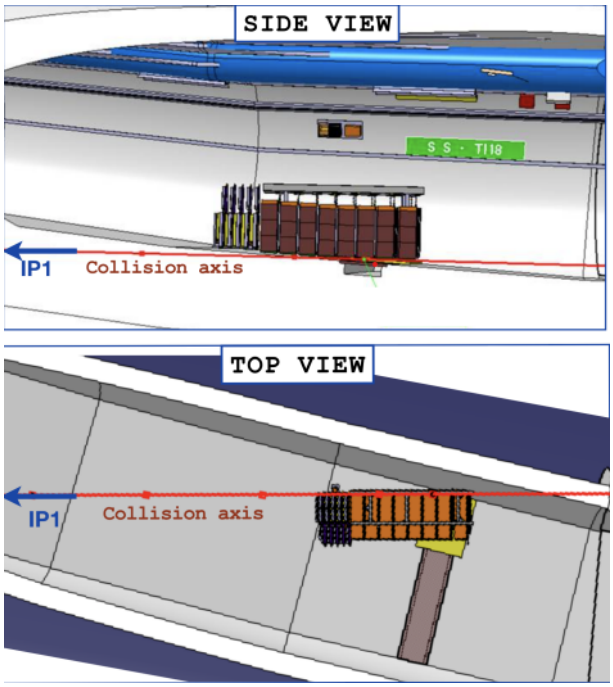

Figure 3.2: SND@LHC detector side and top views in the TI18 tunnel. From [4].

3.1 The SND@LHC apparatus

The SND@LHC apparatus can be split into three main parts: The Veto System (VS), the Emulsion Target (ET) and Scintillating Fiber (SciFi) tracker and the Muon System/Hadronic Calorimeter (MS/HC). The full detector can be seen in Figure 3.3.

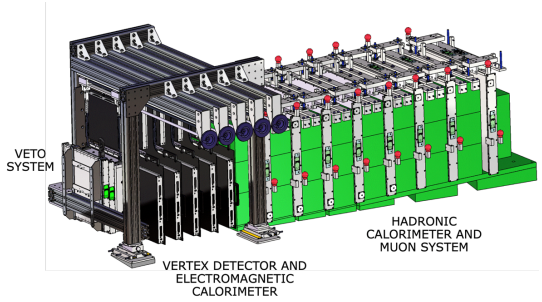

Figure 3.3: SND@LHC detector schematic

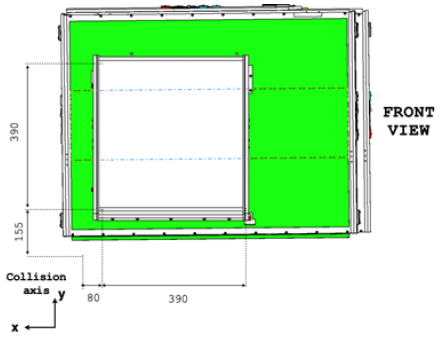

Figure 3.4: Detector offset from collinearity with the beam direction

3.1.1 Veto System

The first part of the detector is the Veto System. This first subsystem comprises scintillating bars that are read out by silicon photomultipliers (SiPM). These bars are encased in aluminium foil to prevent

light loss and to ensure isolation of each individual bar, and have a dimension of $42 \times 6 \times 1cm^3$. As its name implies, it serves the purpose of signaling events where there are charged particles entering the detector. This provides a much needed way to quickly discard events: the distinction can be made from charged leptons associated with neutrino interactions in the detector and charged leptons that overcame the 100 m of material and the LHC dipole magnets, and made their way into the detector.

3.1.2 Emulsion Target and SciFi

Downstream of the Veto, there is the Emulsion Target. It consists of five emulsion walls, each in turn composed of 4 emulsion bricks, with each brick being composed of 60 emulsion films interleaved with 59 layers of 1 mm tungsten plates. This system aims to create tracks and record the position of charged particles when they pass through the emulsion films. Tungsten was selected due to its high density, making the 830kg target ideal for interacting with particles and inducing events. These films can be later developed to provide crucial information about the trajectory and nature of the interaction that took place. The spatial resolution is of order $50\mu m$. Emulsions contain a large quantity of data (10 to 20 fb^{-1}), making purely time-based distinction of the events they contain impossible. Figure 3.5 shows this subsystem in detail.

As can be seen, the 5 emulsion walls contain slots between them. By slotting SciFi trackers in between these walls, one can add time and spatial information for this section of the detector, which is most necessary for making sense of the emulsion data. Additionally, it can be used to measure the energy of showers as they cross the SciFi plane. Tungsten has a radiation length of approximately 0.35 cm. Our target, which is more than 17 radiation lengths long per wall, can reliably contain a electromagnetic shower. However, since tungsten's hadronic interaction length is 9.95 cm, our target cannot fully contain hadronic showers: the full target is about 3 interaction lengths long. The Hadronic calorimeter function is thus fulfilled by a different subsystem. These 5 SciFi planes are made of SciFi fibres with a diameter of $250\mu m$.

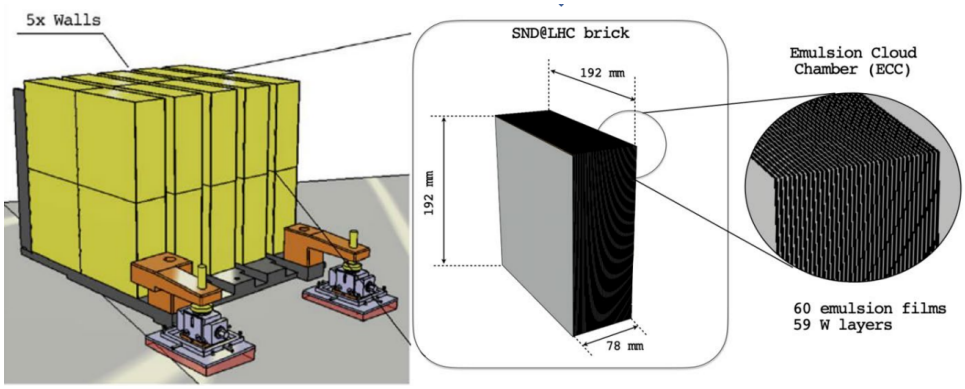

Figure 3.5: SND detector's Emulsion Target composition

3.1.3 Muon System/Hadronic Calorimeter

The last subsystem of the SND@LHC detector is the Muon System/Hadronic Calorimeter. It consists of eight scintillator planes separated by 20cm thick iron blocks, which can be further divided into upstream and downstream planes. The first five planes are named the Upstream (US) planes, and are similar to the Veto subsystem, albeit with different dimensions. Each of these US planes consists of ten horizontal bars, with a dimension of $81 \times 6 \times 1cm^3$. This first planes of the MS/HC lack vertical bars. However, it still retains horizontal resolution by comparing the time between the signals from the right and left sides a bar.

The last three planes, the Downstream (DS) planes, contain a much more granular arrangement of horizontal and vertical bars, which are also shorter than their upstream counterparts: horizontal bars now total 60, with dimensions $81 \times 1 \times 1cm^3$. The vertical bars also total 60 ($60 \times 6 \times 1cm^3$). All of this contributes to a much better spacial resolution. As the name implies, the MS/HC subsystem has two main functions: firstly, it easily identifies muons, which is very important both for neutrino physics and BSM physics. Secondly, it works as an hadronic calorimeter, allowing the detector to measure the energy of hadronic showers. Iron has a hadronic interaction length of 16.77cm. The 8 iron blocks, 9.5 interaction lengths long, combined with the previous subsystems, provide approximately 11 interaction lengths for showers originating in the target.

A side-view of the detector, clearly showing the mentioned layers, can be seen in Figure 3.6. More information on the detector can be verified on the experiment technical proposal [4].

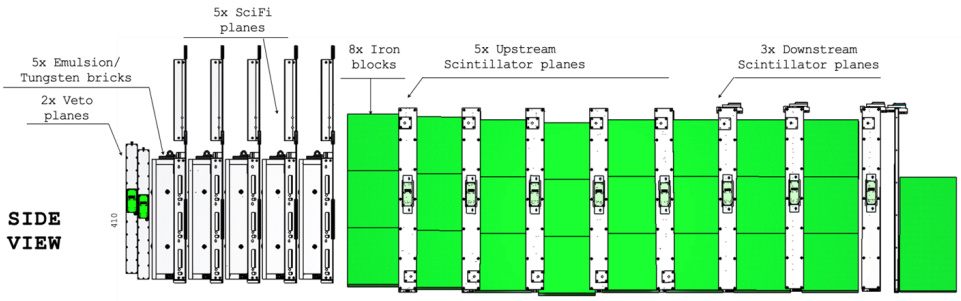

Figure 3.6: Side view of the SND detector

With all these subsystems working together, results are sure to follow: SND@LHC has remarkably already produced a first major physics paper with the first observations of collider muon neutrinos [22]. Moreover, although the current focus of the SND@LHC collaboration is related to detecting and studying collider neutrinos, the experiment was designed with other possibilities in mind, such as the detection and study of Feebly Interacting Particles. SND@LHC's location should make it particularly suitable for these kinds of studies: the near collinearity with the beam guarantees a high luminosity, a very important part on any BSM studies in the intensity frontier. On the other hand, being 480 meters away from the

IP, including 100 meters of solid rock, helps tremendously in reducing the experimental background for this analysis. Moreover, FIP's that tend to decay to heavier particles (like a preference for muons over electrons) would be specially advantageous to SND@LHC analyses over other experiments more suited for lighter decays. This project aims to not only develop the first FIP study at SND@LHC, but test the feasibility of future studies.

4

Signal and Background models

Contents

To generate FIP decay events, the Forward Experiment Sensitivity Estimator (FORESEE) [5,23] was used. This useful tool allows for the simulation of events for various FIPs in "experiments placed in the far-forward direction from the proton-proton interaction point", as is the case for SND@LHC. FORESEE requires us to define our model in detail, including the mass of our FIP, production and mixing methods and allowed decay modes.

4.1 FORESEE simulation settings

No preference was shown to any of the DH production modes presented in the tool. However, only events decaying to muon pairs were analyzed. Although we can ensure only events of this particular decay mode are recorded, it is important to pick a DH mass value where this decay mode would be prevalent. Recalling Figure 2.3, the mass must be set within the range $2m_\mu < m_\phi < 2m_\pi$ or $211.3MeV < m_\phi < 269.9MeV$ (where the mass of two π^0 was considered, since this particle is lighter than its charged counterparts). The chosen mass was $251.2MeV$, provided from a list of logarithmically evenly distributed discrete values provided by the FORESEE tool.

The script also needs specification of the detector geometry. The values were set to be compatible with the SND@LHC detector: 470 meters to the Interaction Point, with a length where the decay can occur of 20 meters, and a event selection on the x-y plane coherent with the offset depicted in Figure 3.4. This initial decay window can and will be tightened as we study the relevant backgrounds for this study.

4.1.1 Generator output

The events outputted by this generator can be obtained in the form of a .csv file, where each event consists of 3 particles (a FIP and 2 muons). These contain a lot of relevant data, such as the particles PDG codes ($\pm$13 for the muons, 32 assigned to the FIP), momenta p_x, p_y, p_z, masses m and charges q, as well as the event vertex spacetime coordinates v_x, v_y, v_z and v_t.

We can use this generated data to do some analysis even before inputting the event into the experiment framework.

4.2 Preliminary study of FIP event generation results

Before analyzing any data, the unbiased nature of the event generation should be checked. For that purpose, 10^6 DH events were generated. The first sanity checks performed were to ensure the vertex was getting generated in the geometric limits previously set, and that the x-y distribution of the vertices was unbiased. Similarly, the momenta of the particles must also be unbiased. As we can see in Figure 4.1, the data was generated according to the defined limits. The muon momenta distributions were

as expected as well: a peak in the lower momenta followed by a exponential-like tail (z-momenta in Figure 4.2a, similar plots for other coordinates in annex A.1).

However, we can also see some of the limitations imposed by our generator's inability to fully generate the particle as one would like: both the x-y plane vertex distribution and momenta distribution for the decaying particle show a clear preference for some values. This is evident when comparing the momenta histograms (figure 4.2).

Even though the sampling of the XY distribution and DH momenta may be improved in future work, it is sufficient for the initial sensitivity study presented in this work. The muons produced in the decay are indeed emitted in a full range of momenta values. The vertex's z-coordinate (annex A.2) is also unbiased, with a uniform distribution of events across the defined range, which should provide hits in different parts of our detector when simulated. This information should, however, be kept in mind to avoid biased conclusions that could stem from poor vertex x-y plane distribution.

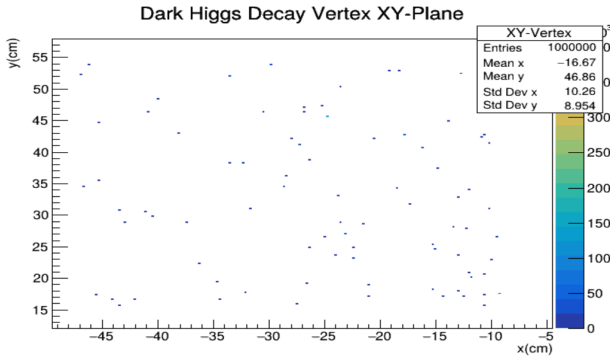

Figure 4.1: XY coordinate distribution for the DH decay vertex

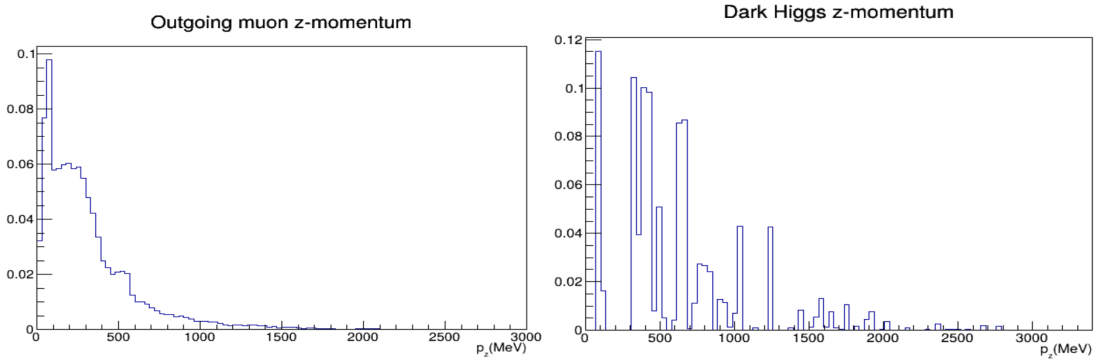

(a) p_z histogram for the outgoing muon

(b) p_z histogram for the decaying FIP

Figure 4.2: Comparison of p_z histograms between DH and outgoing muons (histogram (b) reveals a clear bias in the momentum generation for the FIP)

4.3 Study of decay angle

Thinking logically, the easiest way to spot a double muon event would be if to spot two visibly separated reconstructed muon tracks emerging from the decay vertex. The question of how feasible this would be depends on the opening angle between the two muons. Remembering the size of the bars in the downstream part of the detector, we can reach a threshold for minimum separation of the two tracks. An opening angle of approximately 0.01 radians would result in a $2cm$ separation after $2m$ of detector, leaving hits on multiple bars in the same downstream plane. For angles smaller than this threshold, it would be hard to discern two tracks in the SND detector.

It is possible to obtain the maximum opening angle in the decay of a M mass particle into two m mass particles ($M > 2m$) using the lab frame momentum of the decaying particle. As such we could test if our simulation conditions would allow us to study the dimuons as 2 distinct tracks. In the center of momentum frame:

$$\begin{pmatrix} E_\phi \\ p_{\phi_z} \\ p_{\phi_t} \end{pmatrix} = \begin{pmatrix} M \\ 0 \\ 0 \end{pmatrix} \qquad \begin{pmatrix} E_\mu \\ p_{\mu_z} \\ p_{\mu_t} \end{pmatrix} = \begin{pmatrix} \frac{M}{2} \\ \pm A\cos\theta_z \\ \pm A\sin\theta_z \end{pmatrix} \qquad A = \sqrt{\frac{M^2}{4} - m^2} \tag{4.1}$$

where E, p_z and p_t are the energy, z-momentum and transverse momentum of the particles involved, θ_z is the angle of the momentum of one outgoing muon with the z axis, M and m are the masses of the DH and the muon respectively, and the $\pm$ symbol shows the difference between each of the outgoing muons. These expressions can be confirmed to abide by energy and momentum conservation laws.

By using the Lorentz Boost matrix for a boost along the z-direction:

$$\begin{pmatrix} E' \\ p'_z \\ p'_t \end{pmatrix} = \begin{pmatrix} \gamma & \beta\gamma & 0 \\ \beta\gamma & \gamma & 0 \\ 0 & 0 & 1 \end{pmatrix} \begin{pmatrix} E \\ p_z \\ p_t \end{pmatrix} \tag{4.2}$$

where the primed terms relate to the lab frame, $\beta = \frac{v}{c}$ is the boost and $\gamma = \frac{1}{\sqrt{1-\beta^2}}$, one can obtain the new 4-momenta:

$$\begin{pmatrix} E'_\phi \\ p'_{\phi_z} \\ p'_{\phi_t} \end{pmatrix} = \begin{pmatrix} \gamma M \\ \beta\gamma M \\ 0 \end{pmatrix} \qquad \begin{pmatrix} E'_\mu \\ p'_{\mu_z} \\ p'_{\mu_t} \end{pmatrix} = \begin{pmatrix} \frac{\gamma M}{2} \pm \gamma A\cos\theta_z \\ \frac{\beta\gamma M}{2} \pm A\cos\theta_z \\ \pm A\sin\theta_z \end{pmatrix} \tag{4.3}$$

So, with the lab frame momentum and Mass of the DH, we can calculate the boost and use it to get the opening angle between the dimuon momenta in the lab frame, using the opening angle formula for two momenta p1 and p2 with opening angle α:

$$p1 \cdot p2 = |p1||p2|\cos\alpha \Leftrightarrow \alpha = \arccos\frac{p1 \cdot p2}{|p1||p2|} \tag{4.4}$$

Figure 4.3 shows a plot of the region where pairs of DH mass and lab frame momentum result in an opening angle above or below the threshold set for detector sensibility. For the chosen mass of $251.2MeV$, the momentum would have to be below $39GeV$.

Remembering the detector acceptance from Figure 3.4 to obtain a maximum offset of 10^{-3} radians with the beam collinearity ($54.5cm$ of offset over $480m$ at most), we can now turn our attention to Figure 4.4, which showcases the production of Dark Higgs of mass $251.2MeV$ modeled by FORESEE, as a function of on lab frame momentum and angle with respect to the collision axis. From it, we see that, at 10^{-3} radian offset, Dark Higgs have a minimum lab frame momentum of around $1TeV$, which sets our opening angle to far below the necessary to discern two tracks.

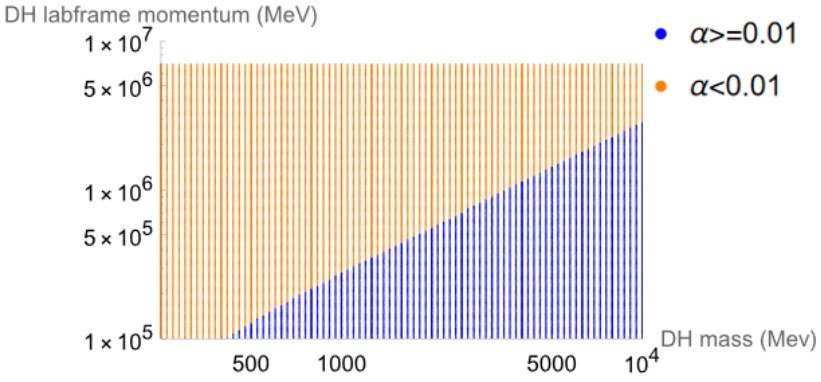

Figure 4.3: Opening angle of outgoing dimuon depending on Dark Higgs mass and lab-frame momentum

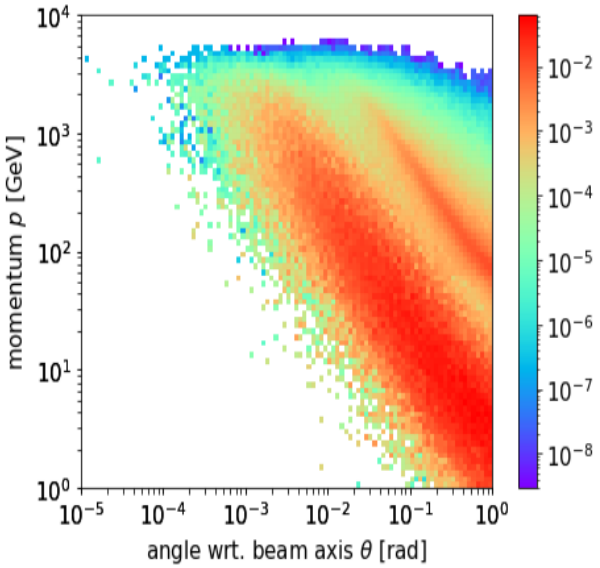

Figure 4.4: Production of Dark Higgs of mass=$251.2MeV$ dependent on lab-frame momentum and angle deviation with beam collinearity

4.4 Relevant backgrounds

Now that we know how our detector will react to the DH decay, it is important that we establish which background events are most likely to interfere with our signal selection to this analysis. Let us follow an hypothetical signal event: a Dark Higgs enters the detector through the Veto acceptance region, leaving no hits. It then decays into 2 muons, perceived collinear by the detector. Muons are notoriously easy to identify in a experimental setting: a clean track penetrating the whole detector, leaving hits as it passes. A simplified drawing of this can be found in Figure 4.5.

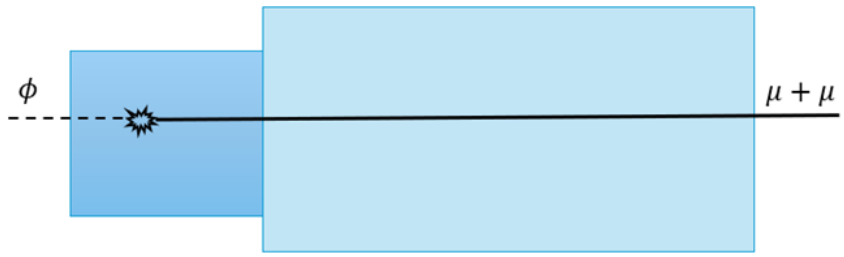

Figure 4.5: Simplified drawing of a DH signal event. Dashed lines are ”invisible” to the detector.

Focusing on the clean track and lack of Veto hits, two main backgrounds emerge: single muons and neutrino interactions. Muons cross the detector very often, usually being discarded because of their Veto hits. Unfortunately, the Veto installed in the SND@LHC apparatus has an inefficiency of 2.5×10^{-6} [24], which occasionally does not trigger with the passage of a muon. This would make it look very similar to a signal event. On the other hand, a muon neutrino can traverse the veto without triggering the Veto, then interact with the detector emitting a muon and other decay products. If these other products have sufficiently low penetration in the detector, it would look like a muon appeared out of nowhere inside the detector, similarly to our signal events. Figure 4.6 shows the simplified drawings for these backgrounds.

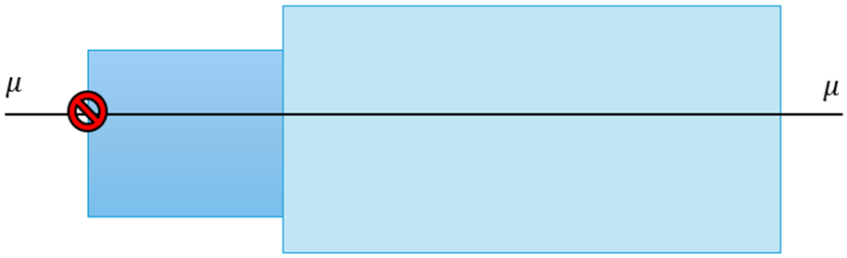

(a) Single muon background

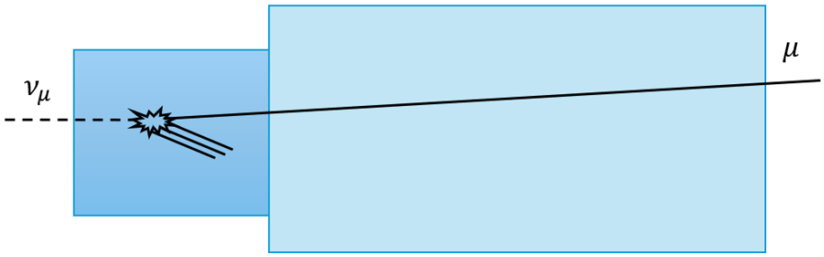

(b) Neutrino interaction background

Figure 4.6: Simplified drawings of background events. Dashed lines are ”invisible” to the detector.

Just like the signal simulation is handled by FORESEE, it is equally important to have a set of MC data for our most relevant backgrounds.

The muon simulation consists on simulating the whole process from the proton-proton collision to the muon propagation and finally interaction with the SND@LHC detector. The proton-proton collision was handled with DPMJET (Dual Parton Model) [25]. Next, the production of muons from said collision was simulated with FLUKA [26]. The propagation of the muon on its way to the detector was also handled with FLUKA, using its LHC model [27]. Finally the interaction with the apparatus was also simulated using SNDSW, similarly to our FORESEE Dark Higgs events. This framework will be expanded upon in section 4.5.

The neutrino simulation was developed largely with the same tools. The proton-proton collision with DPMJET and the propagation with FLUKA are similar to the muon simulator. Neutrino interactions with the detector material were simulated with GENIE [28].

4.5 Event data conversion to SNDSW-compatible format

SNDSW [29] is the software framework of the SND@LHC collaboration. It is based on the FairShip [30] framework developed by the SHiP collaboration which in turn is based on FairRoot, making use of the automatic python bindings provided by PyROOT [31]. To simulate the detector, and interaction of particles with said detector, this framework uses Geant4 [32] (Geometry and Tracking), a software toolkit

developed by CERN for the simulation of the passage of particles through matter. Additionally, SNDSW also contains various other useful scripts utilizing the capabilities of the framework for purposes beyond simulation, such as extrapolating particle tracks from hits in the detector utilizing a Hough Transform approach, or elaborating event displays for a better visual interpretation.

To simulate events in SNDSW one must supply the framework with the generated particle data, so that the script can use that information, in addition to its own knowledge of the SND@LHC apparatus geometry and materials, to simulate how those particles would interact with the detector. One of the formats compatible with SNDSW is the gst ROOT TTree, which contain all the essential data branches, as shown in Figure 4.7.

```
fTree->SetBranchAddress("Ev",&Ev);    // incoming neutrino energy
fTree->SetBranchAddress("pxv",&pxv);
fTree->SetBranchAddress("pyv",&pyv);
fTree->SetBranchAddress("pzv",&pzv);
fTree->SetBranchAddress("neu",&neu);    // incoming neutrino PDG code
fTree->SetBranchAddress("cc",&cc);      // Is it a CC event?
fTree->SetBranchAddress("nuel",&nuel);  // Is it a NUEEL event?
fTree->SetBranchAddress("vtxx",&vtxx);  // vertex  in SI units
fTree->SetBranchAddress("vtxy",&vtxy);
fTree->SetBranchAddress("vtxz",&vtxz);
fTree->SetBranchAddress("vtxt",&vtxt);
fTree->SetBranchAddress("El",&El);      // outgoing lepton momentum
fTree->SetBranchAddress("pxl",&pxl);
fTree->SetBranchAddress("pyl",&pyl);
fTree->SetBranchAddress("pzl",&pzl);
fTree->SetBranchAddress("Ef",&Ef);   // outgoing hadronic momenta
fTree->SetBranchAddress("pxf",&pxf);
fTree->SetBranchAddress("pyf",&pyf);
fTree->SetBranchAddress("pzf",&pzf);
fTree->SetBranchAddress("nf",&nf);     // nr of outgoing hadrons
fTree->SetBranchAddress("pdgf",&pdgf);     // pdg code of hadron
```

Figure 4.7: gst tree branches required for event simulation

But this framework is made to work with neutrino events: it expects an incoming neutrino, outgoing matching flavor charged lepton and some other particles, like hadrons. It is, however, possible to adapt these variables for use in FIP studies: The FIP energy and momenta took the place of the incoming neutrino's and data on the muon pair was slotted into the outgoing hadronic momenta. The outgoing lepton momentum 4-vector is actually not utilized in the simulation of this project, but the FIP data was still duplicated here to prevent any null value errors in the simulator. Finally, the correct PDG codes were introduced and the cc and nueel flags were set to False.

A python script was elaborated to convert the values from the FORESEE csv file to the gst TTree, with the need to calculate the particle energy easily solved by using the equation $E^2 = p^2 + m^2 = p_x^2 + p_y^2 + p_z^2 + m^2$.

This allowed the first FIP events to be simulated in the detector, producing hits in different subsystems like the Target and Muon System (figure 4.8).

From these displays, we can confirm our hypothesis that only DH decays happening a long distance upstream of the apparatus could ever hope to leave two discernible tracks on the detector (since the opening angle threshold would be less demanding). However, these muons would leave hits in the Veto System, making the task of eliminating the background events much more difficult. For DH decays happening in the MS/HC subsystem, our analysis would not be able to rely on the subsystems further Upstream than the decay vertex, like the SciFi. As such, for the remainder of the project, we will be analysing events of DH decays in the Target, defined as a z-range of $[2.8, 3.5]\,m$.

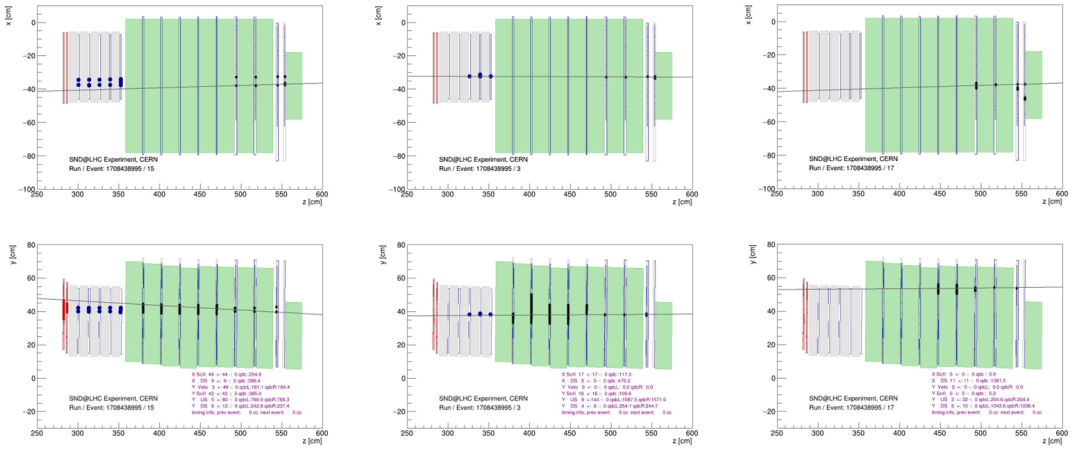

(a) event display of a DH decay before the detector

(b) event display of a DH decay in the target subsystem

(c) event display of a DH decay in the MS/HC subsystem

Figure 4.8: Event displays of various DH decays with different vertex coordinates relative to the detector

5

Event selection and reconstruction

Contents

Now that we have both our signal and background are well defined, we can proceed with the analysis. Before applying any selection to run data events, it is crucial to study the MC simulations of the data samples. This allows for the design of selection cuts with the aim of preserving as much signal as possible, while simultaneously removing enough background as to expect less than one event over the analyzed integrated luminosity. In the particular case of FIP studies, this need for selection is even more pressing: a FIP event is, by definition, extremely rare. On the other hand, a background muon event is very common. Even considering only muons that take advantage of the Veto inneficiecy, it is still a much more common occurrence than a FIP event would be.

5.1 Event features

Each event containing interactions between particles and the detector (be it a run data event or digitized MC simulation) contains a large tree full of event features which can give us specific information when designing the selection cuts.

Firstly, each hit is associated to the subsystem where it was recorded, making it possible to discern hits from the Veto, SciFi, Upstream and Downstream separately. Moreover, the information on the hit placing can be even more particularized, referencing the specific plane and bar the hit took place at. This is very useful, since selection criteria applied to the event hits will naturally differ depending on positioning. Additionally, by cross-referencing this hit with the geometry of the detector, one can obtain the approximate spatial coordinates of the hit.

Each hit also has 2 important data features associated: a QDC (Charge-to-Digital Converter) value and the hit time. The hit QDC, after detector calibration, can be used to infer the energy deposited by the particle when leaving the hit.

Additionally to these initial event features, one can run additional scripts to provide important tools for selection, the most prominent one being the aforementioned muon track recognition script, which utilizes the Downstream hits to identify straight-line tracks, in an attempt to map the muon (in our case, dimuon) path.

5.2 Fiducial cuts

Not all background sample events, be them MC simulation or run data, need complex cuts to discard. A number of simple, fiducial cuts can go a long way.

The first is to eliminate any events that, because of particle trajectory or any other criteria, barely scraped the detector (left too small of an amount of hits) or missed the detector entirely. Additionally, events resulting of simple electronic malfunction or noise are also easily eliminated. This first cut is

simply requiring that the event information is enough such that a track is recognized and reconstructed by the muon track recognition software. This might seem trivial, but it helps eliminate a lot of single muon MC events generated outside our detector's acceptance. This dwindles our sample from 1.1 million initial events to a much smaller sample of around 24 thousand events (2% of the original). Since we can define the volume where the Dark Higgs decay vertex is and force it to be within the detector acceptance, the signal sample is much less affected by this cut (retaining about 98% of events)

All further cuts will be applied only to this approved dataset. The next major cut is, without exaggeration, the main reason a study like this can exist: demanding no hits on the Veto subsystem. This is the main cut that separates muons originating outside the detector and muons from decays inside the detector. Once again, our signal sample maintains almost all events (99.9%) but the single muon MC sample only gets reduced to 50.1%. Since we know the Veto inefficiency is not that severe, we can infer that some muons from the single muon background sample are leaving hits in the Downstream detector despite not crossing the Veto. This is not surprising, since the the Veto has a smaller cross-section than the MS: only about 45% of the MS cross-sectional area, which is where the value for this cut's efficiency roughly comes from. The next step is to reduce this as much as possible.

One approach involves using the track made in the Downstream, and prolonging it to the Veto. This can be done mathematically, since the track as a defined start-point and 3-momentum: by providing the intended z-coordinate, the x and y coordinates will be extrapolated using the equation set:

$$\begin{cases} x = T_x - k * T_{px} \\ y = T_y - k * T_{py} \end{cases} \quad k = \frac{T_z - z}{T_{pz}} \tag{5.1}$$

where (x, y, z) is the extrapolated point, (T_x, T_y, T_z) is a track point, (T_{px}, T_{py}, T_{pz}) is the track 3-momentum and k is the momentum scaling factor. This allows us to demand that the track extrapolation to the Veto z-coordinate (taken $z = 280cm$) be inside the x-y window of the veto. To be sure we eliminate any event just barely passing the detector at the edges, an additional $2.5cm$ border was taken from the initial x-y window. Individually, this cut keeps 23% of the single muon MC background sample and 64% of the signal MC sample. If we put these cuts together, the 24 thousand event background sample dwindles to only 3 surviving events, which is a sign of how vital the Veto is for this analysis. The signal maintained 64.83% of its sample.

With the preliminary cuts out of the way, we can now design more complex cuts to cater to specific backgrounds.

5.3 Additional cuts

5.3.1 Single Muon MC based cut: SciFi cut

After printing some event displays, a problem emerged: some tracks were being extrapolated to the Veto, but from looking at the individual hits, it was evident that the particle was not crossing the Veto (figure 5.1). This comes from the fact that the tracking script only uses the Downstream hits, making the tracks sometimes unreliable.

To combat this flaw, one could set a maximum deviation between SciFi hits and the track extrapolation to the that hit's z-coordinate. But how much deviation should be allowed is a free parameter which can be optimized. To do so, one can compare the maximum deviation of SciFi hits from the track for both the signal MC sample and the single muon MC background sample and use that information to optimize the cut.

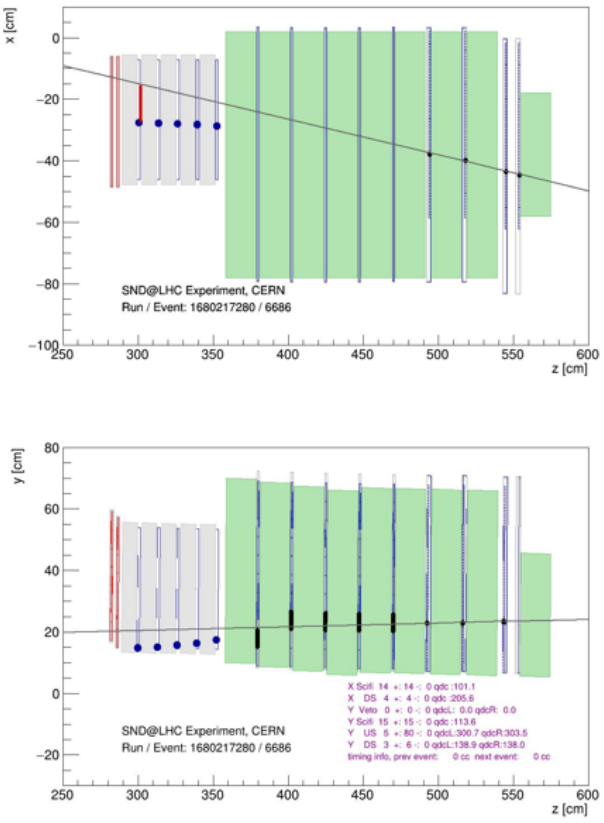

Figure 5.1: Event display from single muon MC background which showcases the shortcomings of a solely-Downstream based track reconstruction

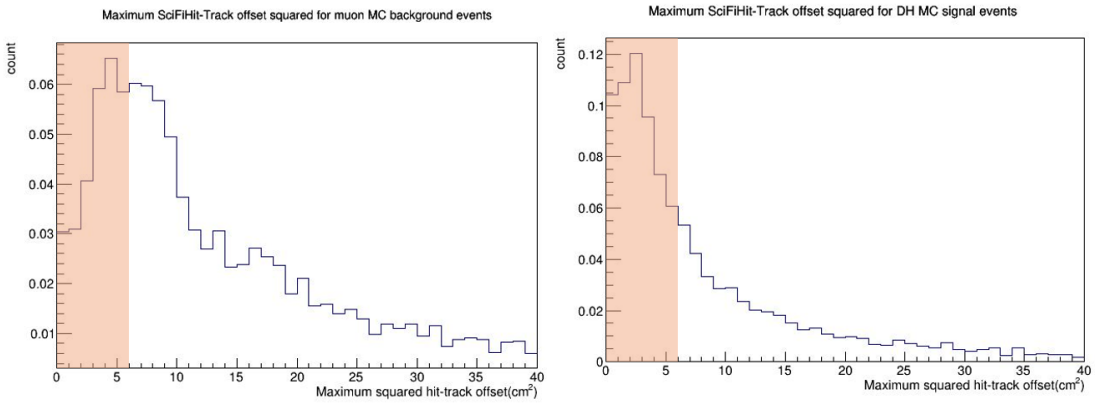

(a) **(b)**

Figure 5.2: Histograms of the maximum squared deviation between SciFi hits and track for the single muon MC (a) and Dark Higgs MC (b) samples. Shaded regions are included in the selection cut.

From the plots in Figure 5.2, we can see that setting the maximum deviation to $\sqrt{5}cm$ on either side allows us to keep a significant part of the signal while reducing a lot of background. Intuitively, given the scale of the detector, a deviation of around $2cm$ makes sense as the threshold for hits ”lining up” with the track.

5.3.2 Neutrino MC based cut: Upstream cut

The selection cuts must be able to reduce most relevant background. This, of course, also includes the neutrino events mentioned in previous sections. Reminding ourselves of the simplified drawing in Figure 4.6b, we might expect more hits per plane for neutrino events compared to our Dark Higgs signal, since a neutrino interaction might produce particle showers in addition to the muon. Comparing both the total amount of hits in the Upstream, as well as the maximum amount of hits in a single plane for the neutrino MC sample and the DH MC sample (figures 5.3 and 5.4), a good opportunity for a selection cut emerges, confirming our intuition. Since we are expecting only one track, the cut should allow at most 2 hits per plane (which should only happen if the muon triggers two adjacent bars). Since there are 5 planes in the Upstream, the DH events should have between 5 and 10 total US hits. To maximize background reduction, the cut was set to only allow event with 5 total hits.

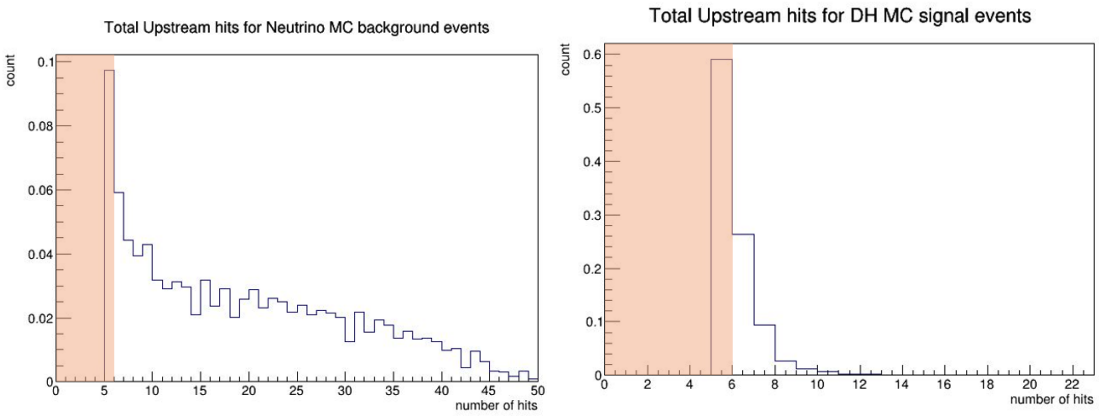

(a) **(b)**

Figure 5.3: Histograms of the total amount of US hits
for the neutrino MC (a) and Dark Higgs MC (b) samples.
Shaded regions are included in the selection cut.

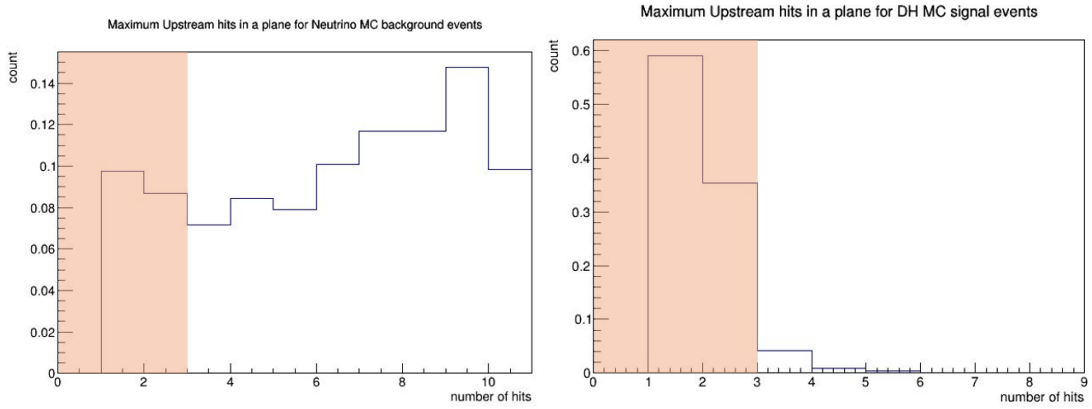

(a) **(b)**

Figure 5.4: Histograms of the maximum amount of US hits in a single plane
for the neutrino MC (a) and Dark Higgs MC (b) samples.
Shaded regions are included in the selection cut.

5.3.3 Run Data-based cuts

After the cuts exhaust our MC samples, the next logical step is to apply them to a small sample of run data events, to check if the data behaves itself similarly to the MC samples. Additionally, it is important to implement some extra cuts that, while redundant when dealing with the simulation, become very important when faced with real events. For our particular case, it is important to restrict the track angle, to ensure that our particles originate from the desired IP. It is also important to implement some quality control cuts to make sure the sample we are studying has no underlying issues. In particular, the time interval between events must be sufficiently large (at least 100 clock-cycles) as to prevent issues related

with dead-time: time that some detectors, such as the Veto, take to become sensitive to a new hit after the previous one.

The range of allowed track angles was once again decided by comparing the signal MC sample with the run data sample which, being only 5 million events large, can be assumed to be fully background. The histograms in Figures 5.5 and 5.6 help us set these limits to $|\theta_{XZ}| < 0.02rad$ and $|\theta_{YZ}| < 0.01rad$.

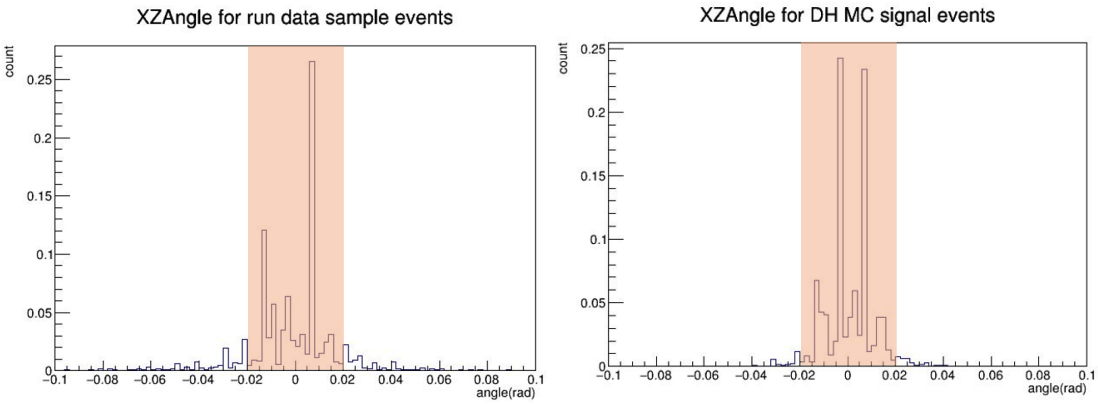

(a) **(b)**

Figure 5.5: Histograms of the XZ track angle for the run data (a) and Dark Higgs MC (b) samples. Shaded regions are included in the selection cut.

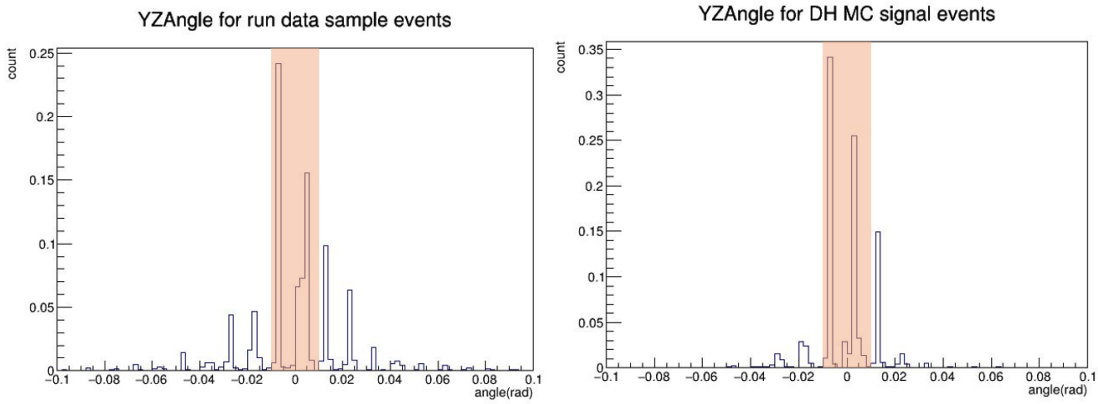

(a) **(b)**

Figure 5.6: Histograms of the YZ track angle for the run data (a) and Dark Higgs MC (b) samples. Shaded regions are included in the selection cut.

5.4 Selection efficiencies

After applying all these cuts, it is important to see their effect on the different samples. Table 5.1 shows both the signal selection efficiency and background survival percentage for the cuts introduced in the

previous subsections. The uncertainty for an efficiency ε, obtained from selecting X events from a total sample of Y is, using error propagation:

$$\sigma_\varepsilon = \sqrt{\left(\frac{\varepsilon(1-\varepsilon}{Y}\right)} \tag{5.2}$$

As we can see, the combination of these cuts exhausted most of our background MC samples while retaining a decent percentage of the signal sample. Additionally, the remaining percentage for the run data sample is actually inferior to the veto inefficiency (2.5×10^{-6}). The neutrino background, when extrapolated to $200fb^{-1}$, comes out to < 0.2 events. This give us some margin to relax our cuts if we want a larger selection efficiency for our signal in the future. For now we move on to another possible way to distinguish between signal and background: the QDC of the hits.

Signal Dark Higgs MC	
Selection cut	**Cut Selection Efficiency**
Reconstructed Track cut	$97.93\% \pm 0.14\%$
Veto cut	$97.81\% \pm 0.14\%$
XY cut	$63.56\% \pm 0.48\%$
Fiducial cuts (track+veto+XY)	$63.49\% \pm 0.48\%$
Fiducial+SciFi cut	$22.11\% \pm 0.42\%$
Fiducial+US cut	$26.67\% \pm 0.44\%$
Fiducial+Angle cut	$37.29\% \pm 0.48\%$
All cuts	$15.36\% \pm 0.36\%$
Backgrounds Single Muon MC	
Selection cut	**Surviving event percentage**
Reconstructed Track cut	$2.17\% \pm 0.013\%$
Veto cut	$1.08\% \pm 0.010\%$
XY cut	$0.50\% \pm 0.006\%$
Fiducial cuts (track+veto+XY)	$(2.7 \pm 1.57) \times 10^{-4}\%$
Fiducial+SciFi cut	$< (9.0 \pm 9.0) \times 10^{-5}\%$
Fiducial+US cut	$(1.8 \pm 1.28) \times 10^{-4}\%$
Fiducial+Angle cut	$(1.8 \pm 1.28) \times 10^{-4}\%$
All cuts	$< (9.0 \pm 9.0) \times 10^{-5}\%$
Backgrounds Neutrino MC	
Selection cut	**Surviving event percentage**
Reconstructed Track cut	$14.8\% \pm 0.37\%$
Veto cut	$14.72\% \pm 0.37\%$
XY cut	$3.26\% \pm 0.19\%$
Fiducial cuts (track+veto+XY)	$2.98\% \pm 0.18\%$
Fiducial+SciFi cut	$< (0.1 \pm 1.0) \times 10^{-3}\%$
Fiducial+US cut	$0.32\% \pm 0.06\%$
Fiducial+Angle cut	$0.90\% \pm 0.10\%$
All cuts	$< (0.1 \pm 1.0) \times 10^{-3}\%$
Run data Run 5396 files 20-24	
Selection cut	**Surviving event percentage**
Reconstructed Track cut	$34.13\% \pm 0.50\%$
Veto cut	$16.06\% \pm 0.38\%$
XY cut	$9.03\% \pm 0.30\%$
Fiducial cuts (track+veto+XY)	$0.038\% \pm 0.020\%$
Fiducial+SciFi cut	$(0.8 \pm 9.3) \times 10^{-4}\%$
Fiducial+US cut	$0.032\% \pm 0.018\%$
Fiducial+Angle cut	$0.008\% \pm 0.009\%$
All cuts	$(0.2 \pm 4.7) \times 10^{-4}\%$

Table 5.1: Signal selection efficiency and Background survival percentage for various selection cuts

5.5 QDC studies

So far, the selection was focused on the existence or absence of hits in certain subsystems of the detector, as well as those hits' quantity and position. But the quality of the hit can also be used for selection, using the QDC value of each hit. Since the hits produced in a signal event would come from two collinear muons instead of just one, the hits in these events could have a larger QDC than most, since the hit QDC is proportional to the energy deposited in the detector.

5.5.1 Minimum QDC in the Upstream

The first approach to QDC studies taken in this project was the following: we consider the closest hit to the reconstructed track in each Upstream plane, and then check for the minimum QDC in those 5 hits. This approach, though simplistic, should reveal if this idea is worth exploring further. An explanation for this method, which will be refered to as "MinQDCUS" (short for Minimum QDC in the Upstream) can be seen in Figure 5.7.

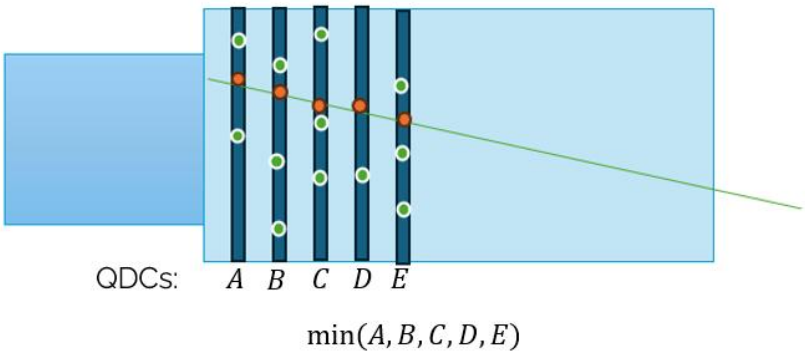

Figure 5.7: Diagram explaining the MinQDCUS method: In the diagram, we can see a simplified detector with the 5 US planes, an event with multiple hits per plane and the reconstructed track. The algorithm takes each US planes' closest hit to the track, and then returns the smallest of the 5 QDCs.

To check our hypothesis, three samples were tested: the single muon MC sample, the Dark Higgs signal MC sample, and a new artificial sample named mock-dimuon MC. This new sample, exclusively used for QDC studies, comes from overlaying two events as if they happened simultaneously, with the QDC associated to each Upstream plane for the mock dimuon equaling the sum of the QDCs from both single muon MC events for that plane. Figure 5.8 shows a diagram explaining the mock-dimuon sample

in the context of MinQDCUS.

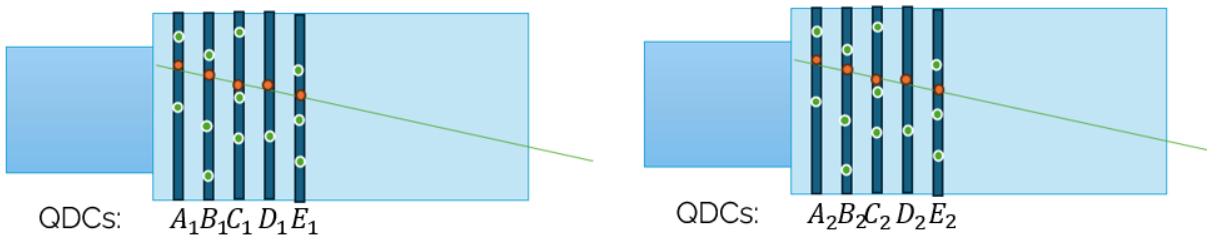

Figure 5.8: Diagram explaining the MinQDCUS method applied to the mock-dimuon sample: In the diagram, we can see simplified detectors with the 5 US planes each, two events with multiple hits per plane and the respective reconstructed tracks. The algorithm takes each US planes' closest hit to the track for each event, and adds then as if they were a single hit in the mock event. It then returns the smallest of the 5 mock QDCs.

Figure 5.9 shows the result of this method for our 3 samples, and the results are very interesting: not only is the peak for the Dark Higgs MC about twice the QDC of the single muon MC, it is also very similar to the mock-dimuon MC profile. If we extend this knowledge to our run data sample, we could estimate the profile for our real DH sample with a run data mock-dimuon.

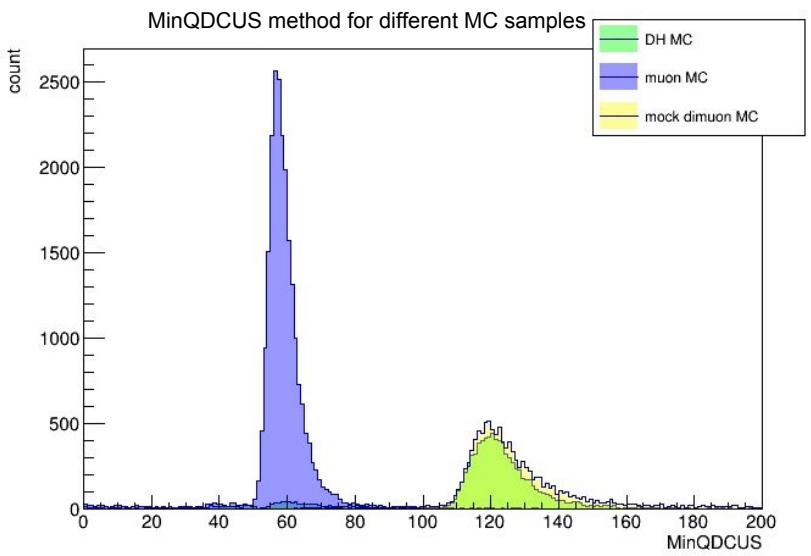

Figure 5.9: Results of the MinQDCUS method for the single muon MC, Dark Higgs MC and mock-dimuon MC samples

Now that we have a strategy to proceed beyond Monte Carlo QDC studies, we should test other methods besides the simplistic MinQDCUS.

5.5.2 Likelihood method

One of the ways that could improve our separation between the regular and mock-dimuon run data samples is the implementation of a likelihood method.

For this new method, the starting selection of the closest hit per Upstream plane would remain unchanged. However, instead of simply selecting the smallest QDC from those 5, the likelihood method would take a slightly more complex approach: two probability density functions (pdfs) would be produced, one with regular hits and one with mock-dimuon hits, prior to the analysis of the event. Each pdf results from merging individual pdfs for each Upstream bar. The most probable value for each individual pdf is calculated, and then a shift equal to the offset between this value and the average most probable value over all pdfs is applied. After shifting all pdfs, they are added. Such calibration results in a more pronounced peak in the total pdf and reduces potential error propagation if there is a technical problem with a limited number of bars.

Now, after an event has its 5 selected hit QDCs, each of those 5 values would be checked for the probability of belonging to each of the pdfs.

By adding the logarithms of these probabilities, we should avoid any computational rounding errors and get a more stable calculation. If the algorithm returns a positive value, the event is overall more similar to a regular (single muon) event. But if a negative value is returned, it would be more likely to be a dimuon event, and thus more signal-like. Figure 5.10's diagrams contains a visual explanation for this method.

5.5.3 Comparison between QDC methods for run data samples

. The two methods mentioned in the previous subsections were applied to both the run-data sample and the mock-dimuon data sample. Plotting both samples in the same graph allows us to see the overlap between the profiles from each methods results.

The profiles for the MinQDCUS and likelihood methods can be seen in Figures 5.11 and 5.12 respectively. As we expected, it is evident that we obtain better separation between our two cases (single muon and dimuon) by using the likelihood method. This is further confirmed by the overlapped ROC curves (figure 5.13). It is worth noting the peculiar profile for the likelihood of the run data sample, something which could be tackled in future work.

This new likelihood method can become a very powerful selection cut if the threshold is set properly. In combination with the veto cut, which we can assume is independent from this method, we are now in a position to estimate our background.

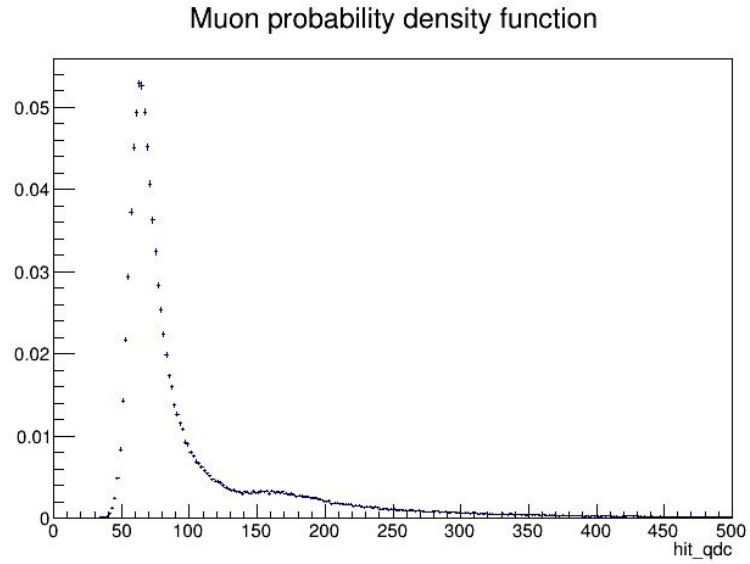

(a)

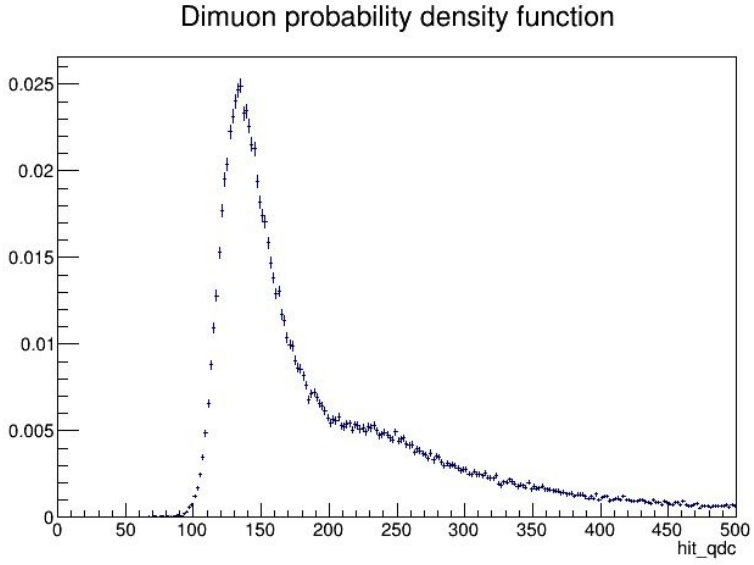

(b)

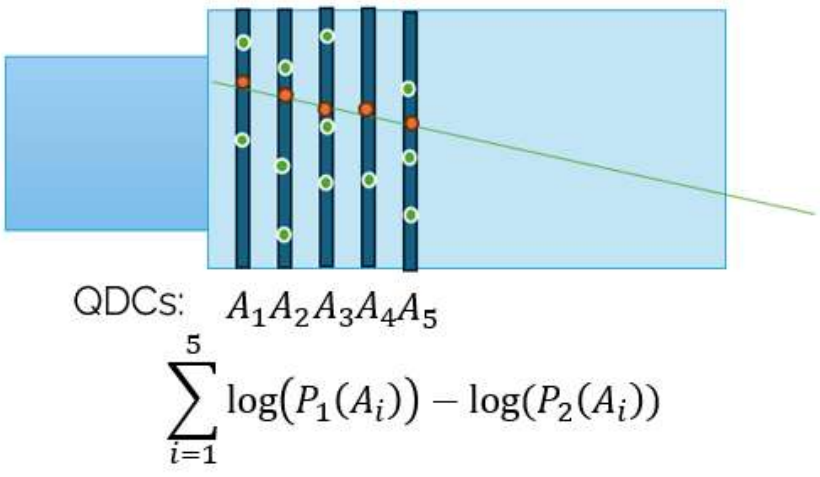

(c)

Figure 5.10: Diagram explaining the likelihood method employed: (c) shows a simplified detector with the 5 US planes, an event with multiple hits per plane and the reconstructed track.
Before the analysis started, a different run data sample was used, and each selected hit (see Figures 5.7 and 5.8 for the selection) was used to fill the two pdfs ((a) and (b)).
Finally, each selected hit from the analyzed event gets its QDC value plugged into the log-likelihood formula, where P_1 and P_2 are the pdfs for single muon and mock-dimuon respectively.

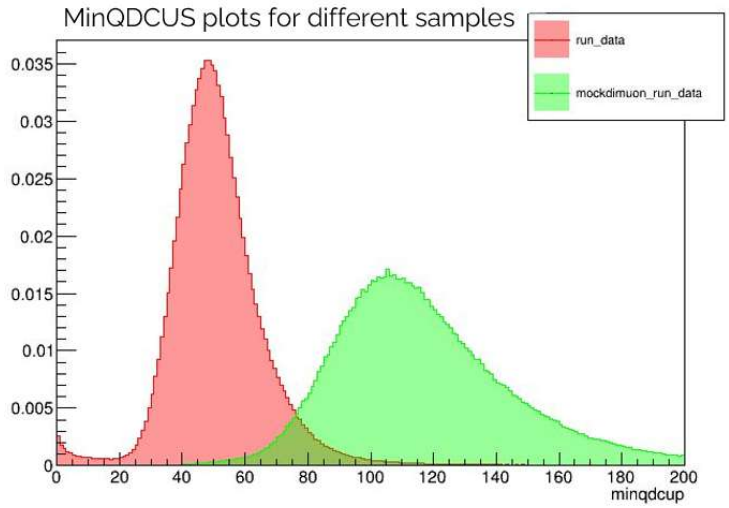

Figure 5.11: Normalized MinQDCUS method results for the run data and mock dimuon data samples

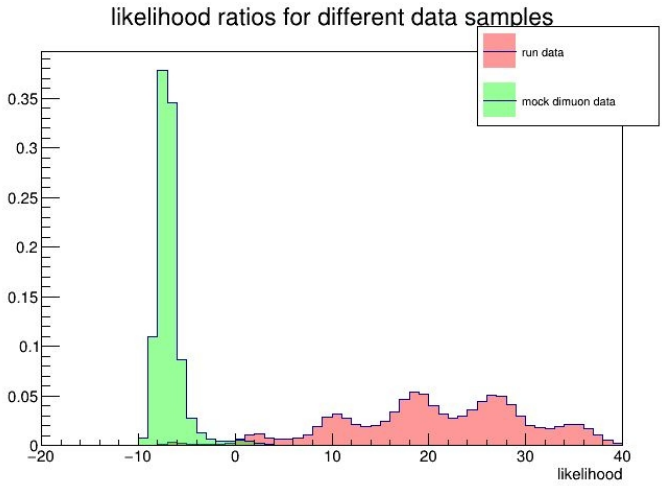

Figure 5.12: Normalized likelihood method results for the run data and mock dimuon data samples

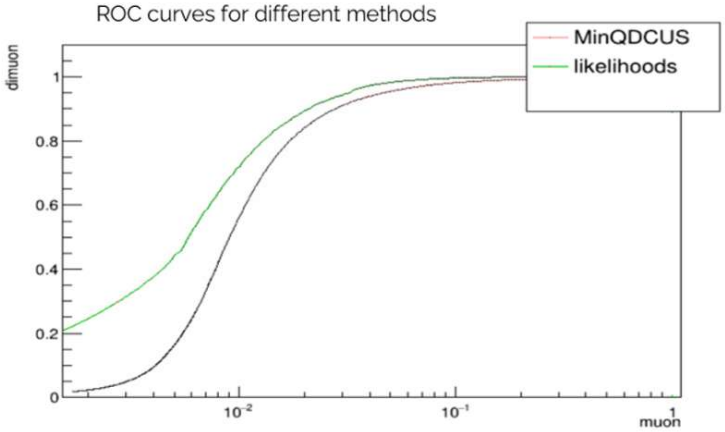

Figure 5.13: ROC curves for the MinQDCUS and likelihood methods

6

Likelihood Threshold Optimization and Background Estimation

Contents

In this chapter, we aim to use our previously studied selection metrics to estimate the background in the signal region. To do so, we will be employing the ABCD method of background estimation [33].

6.1 The ABCD method

The ABCD method is a background estimation method commonly used by many analyses at the LHC searching for new physics [33]. The method requires that two selection metrics that delimit the signal region are chosen subsequently used to define 4 regions according to the data points' agreement with one, both or none of these cuts. For this analysis, the chosen metrics were the presence of Veto hits and the QDC-likelihood developed in subsection 5.5.2 and the regions are outlined in Figure 6.1.

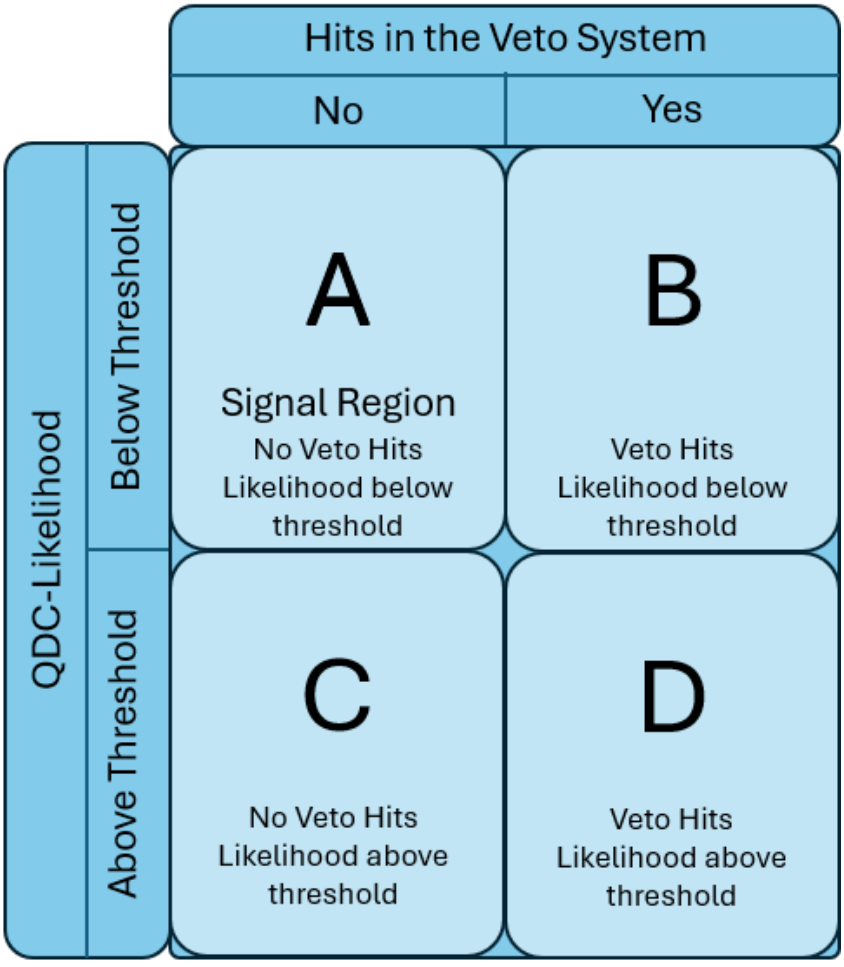

Figure 6.1: Data Regions for the ABCD background estimation method. A is the signal region, while the rest are background regions.

One of the aspects that makes the ABCD method such a preference amongst new physics analyses is the low requirements of its application. For the method to work, the main condition is to make sure

that the two selection metrics chosen are sufficiently uncorrelated for background events. This can be written in equation form as:

$$\frac{N_A^{bkg}}{N_B^{bkg}} = \frac{N_C^{bkg}}{N_D^{bkg}} \tag{6.1}$$

For this analysis, we also assume that all the events in regions B, C and D are background events, since we do not have a reliable prediction for the number of signal events in each of these regions. However, looking at our analysis so far, it is safe to assume that the number of signal events in these regions will be negligible.

One objection could, however be raised: depending on where our likelihood threshold, region C (events with no Veto hits with QDC-likelihood above the threshold) could contain signal events. However, remembering equation 6.3, we see that overestimating the amount of background in C actually leads to a higher background estimation on the signal region. So our prediction will always be a worse-case scenario compared to the true background in the signal region and hence has no risk of yielding a false discovery, though it could reduce the sensitivity of the analysis.

$$N_i^{bkg} \simeq N_i \text{ , for } i = B, C, D \tag{6.2}$$

Reorganizing equation 6.1, we get that our background estimation for the signal region is:

$$N_A^{bkg} = \frac{N_C^{bkg}}{N_D^{bkg}} N_B^{bkg} \simeq \frac{N_C}{N_D} N_B \tag{6.3}$$

6.1.1 Method verification

Instead of just applying the ABCD method for background estimation to our data, it is prudent to check its effectiveness. For that purpose, we can apply it to our single muon MC (a sample which is, by definition, composed of only background events). By comparing the number of events in the signal region (which should all be background for this sample) with the background estimation for that same region for different likelihood thresholds, we should get compatible values.

Applying this test to our single muon MC sample will unfortunately not yield any results. As was seen in section 5.4, even before introducing the QDC-likelihood, there are no events in that pass all selection metrics and lack veto hits. This would effectively leave empty both A and C regions which, while agreeing with equation 6.1, is not a useful result. However, by introducing a large artificial veto inefficiency (50% for our test), we would be able to populate all regions for the sake of confirming the method.

Figure 6.2 compares the expected background in the A-region (signal region) with the real amount of events sorted to that region for different values of the QDC-likelihood threshold. Because we are applying this method to a sample of only background, these two numbers should be compatible if the method can be applied. This seems to be the case, with the A-region event numbers falling within the

standard deviation of the background prediction.

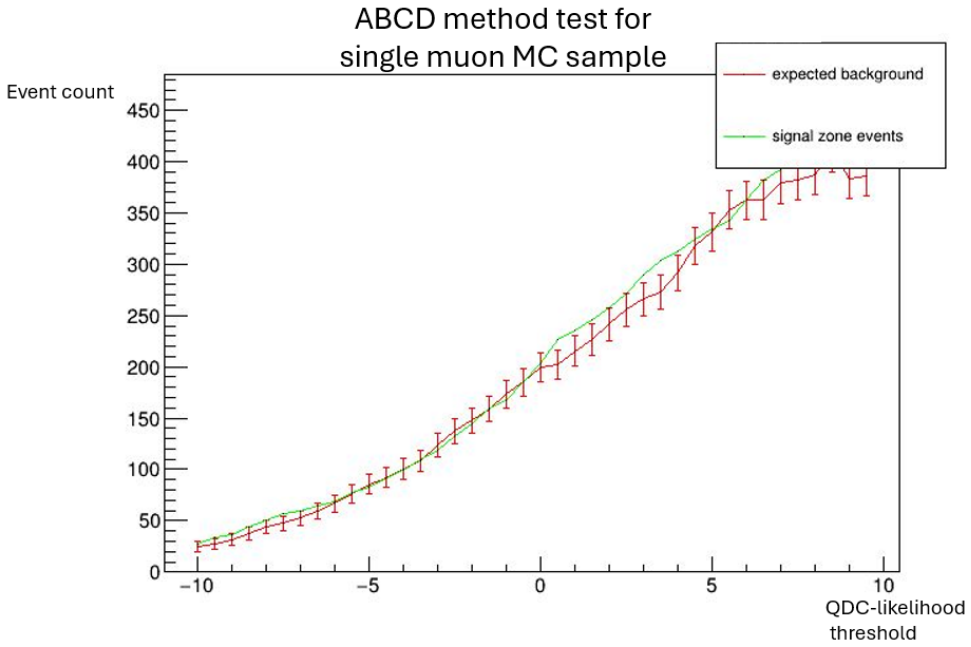

Figure 6.2: ABCD method test applied to the single muon MC sample.
An artificial veto inefficiency of 50% was introduced for the purpose of filling all regions. The error bars in the background estimation represent the standard Poisson distribution deviation.

6.2 QDC-likelihood threshold optimization

Following the successful verification of the method, we can now apply it to run data events. As such, it is imperative that we define a QDC-likelihood threshold such that the signal region contains as little background as possible. To do this rigourously, an optimization metric was devised using the signal selection efficiency for each threshold and the expected background in the signal region assuming the best detector conditions in the 2022-2023 timeframe, presented in Figure 6.3. The optimization formula used was:

$$\frac{\varepsilon_{sig}(\%)}{\sqrt{A_{bkg}}} \tag{6.4}$$

where ε_{sig} is the signal selection efficiency and A_{bkg} is the expected background in the signal region.

The optimization metric for different thresholds is displayed in Figure 6.4. From it, we can define this threshold to have a value of -6. This value gives us a low expected background in the A-region, while also retaining around 83.2% of the signal events. Combining this with our previous selection cuts, our final signal selection efficiency is 12.78%.

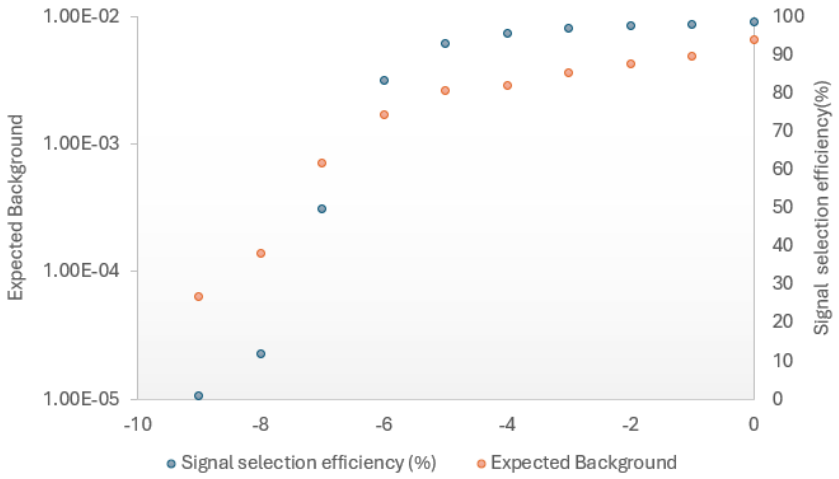

Figure 6.3: Signal selection efficiency ($\%$) and expected background in the signal region for different QDC-likelihood thresholds

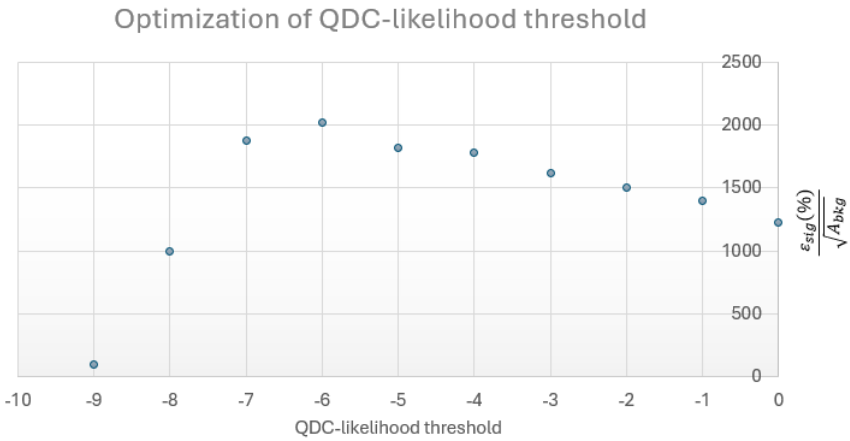

Figure 6.4: Optimization of the QDC-likelihood threshold using the signal selection efficiency (ε_{sig}) and expected background in the signal region(A_{bkg})

6.3 Background Estimation of Run Data

With the ABCD regions set, we move on from our fairly small sample and apply our method to a more significant amount of data. Four run data samples, containing between $0.5fb^{-1}$ and $1fb^{-1}$ each, roughly 100 times the events in our previous sample, were studied in this section. We decided to not yet blind ourselves to the number of events in the A region for each sample. Since this is still a very small fraction of the total luminosity of SND@LHC data, there is no risk of our analysis becoming biased, and we can use the info gained to cross-check the validity of our assumptions, making sure everything looks well with the method predictions.

Table 6.1 shows the ABCD method results for each of the four runs. When choosing which runs to analyse, it was important to validate our method for different data-taking conditions. As such, both run 5000 and run 6079 were chosen from a period of data-taking which had larger Veto inefficiencies than usual, stemming from a temporal misalignment between the Veto system and the other detector subsystems that caused Veto hits to sometimes not be attributed to the event. This is apparent when comparing the number of events with Veto hits passing all pre-ABCD selection cuts (all cuts detailed in chapter 5, excluding the Veto cut). Additionally, to check how well the number of events in the signal region agrees with the expected background in this region, the χ^2 was calculated using the formula:

$$\chi^2 = \frac{(A_{bkg} - A)^2}{A_{bkg}} \tag{6.5}$$

where A is the number of events in the signal region and A_{bkg} is the expected background.

Table 6.2 displays the results of the method extrapolated to $200fb^{-1}$: the background expectation and the minimum number of observed events required to achieve statistical significance of 5 sigma. Note that we are referring to 5 sigma in the usual sense of Gaussian-like exclusion.

Run number	Luminosity(fb^{-1})	B	C	D	A_{bkg}	A	χ^2
5000	0.60	206	114	124475	0.19 ± 0.018	0	0.19
5396	0.79	217	1	124957	0.0017 ± 0.0017	0	0.0017
6079	0.83	19	600	6616	1.72 ± 0.07	1	0.55
6264	0.82	271	2	89887	0.006 ± 0.004	0	0.006

Table 6.1: ABCD method results for 4 run data samples containing: number of events in each of the 4 zones (A,B,C,D); expected background in the signal region (A_{bkg}); Chi-squared test of A in relation to the expected background A_{bkg} (χ^2). The uncertainty of A_{bkg} was calculated using the statistical uncertainty of the expected background, $\sqrt{C}/D * B$

Run number	Luminosity (fb^{-1})	$A_{bkg}(200fb^{-1})$	$N_{5\sigma}$ $(200fb^{-1})$	$N_{5\sigma}/\varepsilon_{sig}$ $(200fb^{-1})$
5000	0.6	63.3 ± 6	107	837
5396	0.79	0.43 ± 0.43	7	54
6079	0.83	414.46 ± 16.87	520	4068
6264	0.82	1.46 ± 0.98	11	86

Table 6.2: ABCD method results extrapolated to $200fb^{-1}$: Expected background in the signal region, minimum events for background-only exclusion at 5σ ($N_{5\sigma}$) and minimum events for background-only exclusion at 5σ divided by signal selection efficiency ($N_{5\sigma}/\varepsilon_{sig}$). The uncertainty of A_{bkg} was calculated using the statistical uncertainty of the expected background, $\sqrt{C}/D * B$

Firstly, it is reassuring to confirm that the number of events in the signal region is compatible with the background expectation (all χ^2 below 1).

We come to the conclusion that, for runs where the Veto is working properly, we achieve a very good selection. Although it is not enough for single-event 5-sigma discovery over the $200fb^{-1}$,for the best run, our selection has a background expectation below 1 even after extrapolation. For the studied runs

with an abnormally inefficient Veto, the expected background proved too large when extrapolated to the $200 fb^{-1}$.

To put these values into perspective, it is important to mention that between 2022 and 2024, SND@LHC recorded $180 fb^{-1}$ worth of data, with around $30 fb^{-1}$ suffering from the Veto misalignment issues. We conclude that, for the best detector conditions, this selection proves to be extremely effective in identifying decay to dimuon events, requiring 7 events in the signal region for background-only exclusion at 5 sigma which, when considering our signal selection efficiency, corresponds to, on average, 54 Dark Higgs decays in the target subsystem.

6.4 Model exclusion

Besides the background-only analysis exclusion, we can utilize our background expectation to draw exclusion regions in the DH model parameter-space. For an exclusion at 90%, we would calculate what the signal expectation needs to be so that seeing only the expected number of background events or lower would account for less than 10% of the Poisson distribution. For our best detector conditions case, the expected background of 0.43 would give us exclusion at 90% for a signal expectation of 2.55 (20 events when the signal selection efficiency is considered). This allows us to draw exclusion regions in the DH phase-space, which are displayed in Figure 6.5 along with previous exclusions made by other collaborations. As can be seen, with the current selection, our analysis is comparable to previous exclusions in the same mass range. However, should we be able to double our signal efficiency (resulting in a signal event decrease from 20 to 10), we would start probing previously unexcluded areas. Revisiting the selection plots of section 5.4, relaxing the track angle cut and maximum total hits in the Upstream cut appear to be promising ways to increase signal selection efficiency.

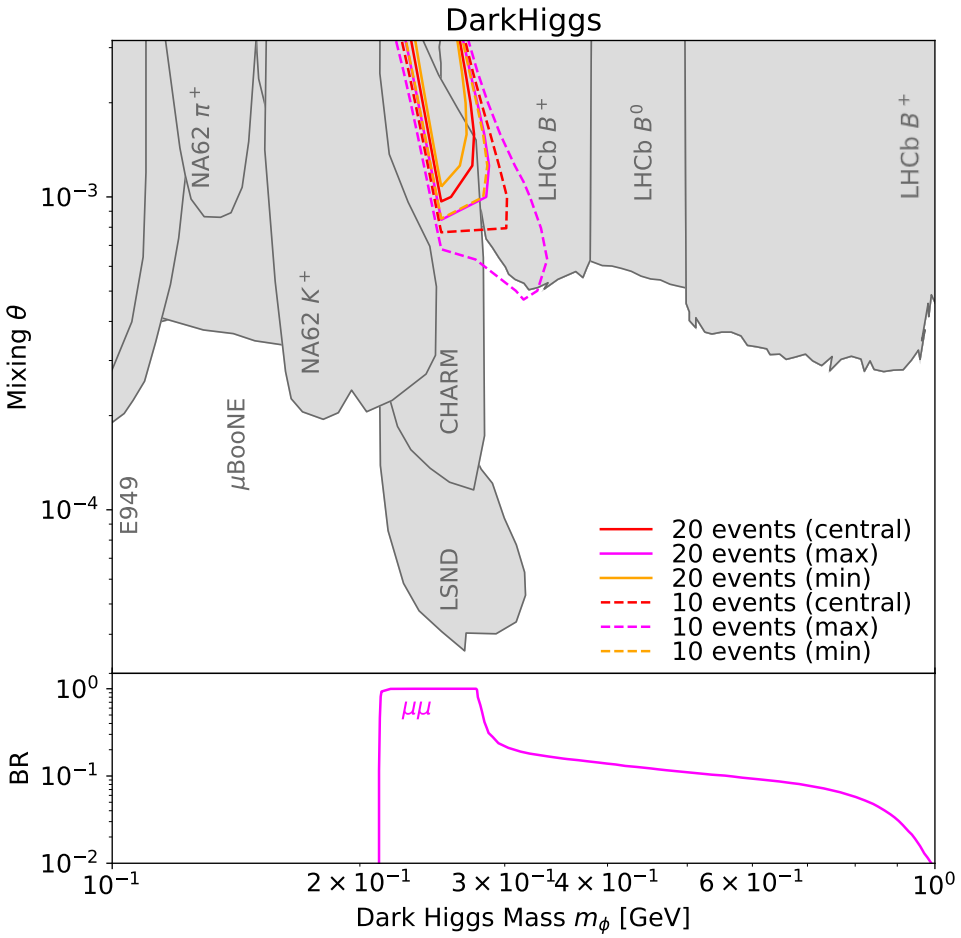

Figure 6.5: Excluded Regions in the Dark Higgs phase space in relation to DH mass and mixing angle. The 3 curves (central, max and min) come from the uncertainty of hadron generation with POWHEG. Colored solid lines correspond to the exclusion based on our current expected background and signal selection efficiency. Colored dash lines correspond to the exclusion should we double our signal selection efficiency. Previous exclusions taken from FORESEE [5].

7

Closing Remarks

Although the Standard Model is a very successful theory, it is not able to explain some of the outstanding problems of modern physics. For these problems, the extension of the SM using BSM physics is required.

The Scattering and Neutrino Detector at the LHC is the latest built experiment at the LHC. It is a compact and stand-alone experiment designed for the observation of collider neutrinos.

In this thesis, the aim was to conduct the first FIP analysis study at SND@LHC. This analysis was signature driven, focusing on the experimental signature of the studied decay mode (decay to dimuon) more than the specific nature of the decaying particle.

The thesis began by providing a theoretical introduction to the Standard Model, with particular emphasis on the Higgs mechanism due to its relation to the project's benchmark particle. This was followed by an introduction to Feebly Interacting Particles (FIPs) before focusing on the Dark Higgs (DH): a particle whose interaction with the SM is done through mixing with the SM-Higgs. We introduced the formalism of this FIP's addition to the SM using the scalar portal framework, as well as its most relevant production and decay modes.

This was followed by an introduction to the SND@LHC experiment, highlighting its potential for FIP studies, both in terms of location and with a system by system overview of the SND@LHC apparatus.

In chapter 4, we focused on the signal and background models, defining the parameters of our signal, such as the DH mass ($251.2MeV$) and vertex coordinates, used in the simulation of our signal Monte-Carlo sample, which was done with the Forward Experiment Sensitivity Estimator (FORESEE [5]). Some preliminary studies were done to verify correct and unbiased event generation. A DH decay angle study also revealed the need to treat the 2 muons as collinear. This collinearity lead to relevant background from single-muon events and neutrino events. Lastly for this section, the signal MC data was converted to a SNDSW-compatible format and, through the analysis of event displays, the decision to focus on DH decays in the target subsystem was made.

Chapter 5 focused on event selection and reconstruction, introducing the various selection cuts developed throughout the project, from fiducial cuts to cuts related to specific data from apparatus subsystems, like the SciFi and the Muon System. Muon track reconstruction also played an important role in background exclusion. Two different QDC-based selections were also studied, with the QDC-likelihood method offering a larger reduction of the single muon background. This chapter also featured a very important result: by combining the hit QDCs of two single-muon MC events to obtain a mock-dimuon MC event, we obtained very similar profiles between the Dark Higgs MC sample and this new mock-dimuon MC sample. We proceeded to extend this knowledge to run data in following chapters, treating this run data mock-dimuon as our signal for the remaining of the thesis.

This thesis finalized with a background estimation using the ABCD method, using the QDC-likelihood and presence of Veto hits in the event as our two uncorrelated selection metrics. An optimization of

the QDC-likelihood threshold was also done, maximizing signal selection efficiency while minimizing expected background in the signal region. Following this, we applied the method to larger data samples from different runs. To validate the method for different conditions, runs with different conditions of Veto inefficiency were used. Our analysis concludes with a signal selection efficiency of 12.78%, a neutrino background of < 0.2 over $200 fb^{-1}$ and an expected muon background for the best detector conditions of 0.43 ± 0.43 over $200 fb^{-1}$. This corresponds to 7 events required for a background-only exclusion at 5 sigma, which in turn corresponds to 54 Dark Higgs decays in the target subsystem. We were also able to exclude mixings of 10^{-3} or higher for our mass range, and predicted access to unexcluded regions should our selection efficiency increase by a factor of 2.

Although this thesis concludes with some very satisfying results, a lot of future work could still be developed for this project. The cuts initially developed could be reoptimized to maximize sensitivity for $200 fb^{-1}$, accounting for the impact of the QDC-likelihood method. In particular, relaxing the track angle cut and maximum total hits in the Upstream cut looks promising. We could also attempt to validate our QDC-likelihood method using data events with two muons passing through the same Upstream bar (and leaving hits in the Veto). The statistics for this kind of event are fairly scarce, but it should be enough for validation. Turning to the theoretical side, we could interpret our results in terms of limits to the parameters of other particle models with dimuon decay modes that might be relevant. Finally, we could actually apply the analysis to all the data acquired by SND@LHC between 2022 and 2024 and later publish our findings.

Bibliography

[1] CERN Courier, "SHIP sets a new course in intensity frontier exploration." Image, 2016. image by Richard Jacobsson and Daniel Dominguez.

[2] J. L. Feng, I. Galon, F. Kling, and S. Trojanowski, "Dark Higgs bosons at the ForwArd Search ExpeRiment," Physical Review D, vol. 97, Mar. 2018.

[3] F. Alicante, "Study of neutrino interactions at SND@LHC," 2023. Presented 22 May 2023.

[4] SND@LHC Collaboration, "SND@LHC - Scattering and Neutrino Detector at the LHC," tech. rep., CERN, Geneva, 2021.

[5] F. Kling and S. Trojanowski, "FORESEE: FORward Experiment SEnsitivity Estimator."

[6] B. Holstein, "The Theory of Almost Everything: The Standard Model, the Unsung Triumph of Modern Physics ," Physics Today, vol. 59, pp. 49–50, 07 2006.

[7] FCC Collaboration, "Future Circular Collider." CERN Project, 2024. Accessed: 2024-08-20.

[8] C. Pralavorio, "SHiP sets sail to explore the hidden sector," 2024.

[9] FASER Collaboration, "FASER: ForwArd Search ExpeRiment at the LHC," 2019.

[10] CMS Colaboration, "Observation of a new boson at a mass of 125 GeV with the CMS experiment at the LHC," Physics Letter B, 2012.

[11] ATLAS Collaboration, "Observation of a new particle in the search for the Standard Model Higgs boson with the ATLAS detector at the LHC," Physics Letter B, 2012.

[12] C. N. Yang and R. L. Mills, "Conservation of Isotopic Spin and Isotopic Gauge Invariance," Phys. Rev., vol. 96, pp. 191–195, Oct 1954.

[13] S. L. Glashow, "Partial Symmetries of Weak Interactions," Nucl. Phys., vol. 22, pp. 579–588, 1961.

[14] S. Weinberg, "A Model of Leptons," Phys. Rev. Lett., vol. 19, pp. 1264–1266, Nov 1967.

[15] G. 't Hooft and M. Veltman, "REGULARIZATION AND RENORMALIZATION OF GAUGE FIELDS.," Nucl. Phys. B44: No. 1, 189-213(1972).

[16] P. Janot and S. Jadach, "Improved Bhabha cross section at LEP and the number of light neutrino species," Physics Letters B, vol. 803, p. 135319, Apr. 2020.

[17] S. Alekhin et al., "A facility to search for hidden particles at the CERN SPS: the SHiP physics case," Reports on Progress in Physics, vol. 79, p. 124201, Oct. 2016.

[18] J. Beacham et al., "Physics beyond colliders at CERN: beyond the Standard Model working group report," Journal of Physics G: Nuclear and Particle Physics, vol. 47, p. 010501, Dec. 2019.

[19] European Strategy for Particle Physics Preparatory Group, "Physics Briefing Book," 2020.

[20] Particle Data Group, "Review of particle physics: CKM Quark-Mixing Matrix," Phys. Rev. D, vol. 110, no. 3, p. 030001, 2024.

[21] B. Grinstein, L. Hall, and L. Randall, "Do B meson decays exclude a light Higgs?," Physics Letters B, vol. 211, no. 3, pp. 363–369, 1988.

[22] S. Collaboration, "Observation of Collider Muon Neutrinos with the SND@LHC Experiment," PHYSICAL REVIEW LETTERS, vol. 131, July 2023.

[23] F. Kling and S. Trojanowski, "Forward experiment sensitivity estimator for the LHC and future hadron colliders," Physical Review D, vol. 104, Aug. 2021.

[24] R. Albanese et al., "Observation of Collider Muon Neutrinos with the SND@LHC Experiment," Physical Review Letters, vol. 131, July 2023.

[25] A. Fedynitch, "Cascade equations and hadronic interactions at very high energies," 2015. Presented 27 Nov 2015.

[26] D. Prelipcean et al., "Comparison Between Run 2 TID Measurements and FLUKA Simulations in the CERN LHC Tunnel of the Atlas Insertion Region," in Proc. IPAC'22, no. 13 in International Particle Accelerator Conference, pp. 732–735, JACoW Publishing, Geneva, Switzerland, 07 2022.

[27] C. Ahdida et al., "New Capabilities of the FLUKA Multi-Purpose Code," Frontiers in Physics, vol. 9, 2022.

[28] C. Andreopoulos, A. Bell, D. Bhattacharya, F. Cavanna, J. Dobson, S. Dytman, H. Gallagher, P. Guzowski, R. Hatcher, P. Kehayias, A. Meregaglia, D. Naples, G. Pearce, A. Rubbia, M. Whalley, and T. Yang, "The GENIE neutrino Monte Carlo generator," Nuclear Instruments and Methods in Physics Research Section A: Accelerators, Spectrometers, Detectors and Associated Equipment, vol. 614, p. 87–104, Feb. 2010.

[29] SND@LHC Collaboration, "SNDSW:SND@LHC experiment framework based on FairShip and FairRoot."

[30] SHIP Collaboration, "FairShip: A Simulation and Reconstruction Framework for SHiP Experiment," 2024. GitHub repository, accessed: 2024-09-02.

[31] R. Brun and F. Rademakers, "ROOT - An Object Oriented Data Analysis Framework." http://root.cern.ch/, 1996.

[32] S. Agostinelli et al., "Geant4—a simulation toolkit," Nuclear Instruments and Methods in Physics Research Section A: Accelerators, Spectrometers, Detectors and Associated Equipment, vol. 506, no. 3, pp. 250–303, 2003.

[33] W. Buttinger", "ABCD Method: Data-driven Background Estimation in High Energy Physics," 2018. Accessed: 2024-10-07.

A

Additional plots and images

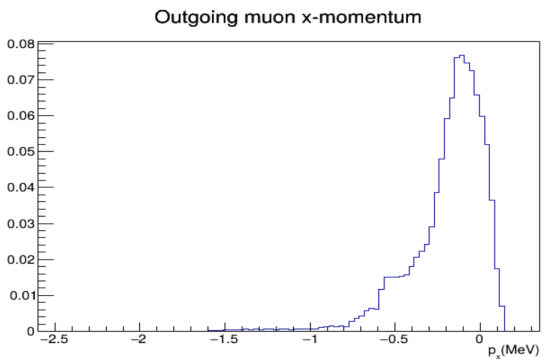

(a) p_x histogram for the outgoing muon

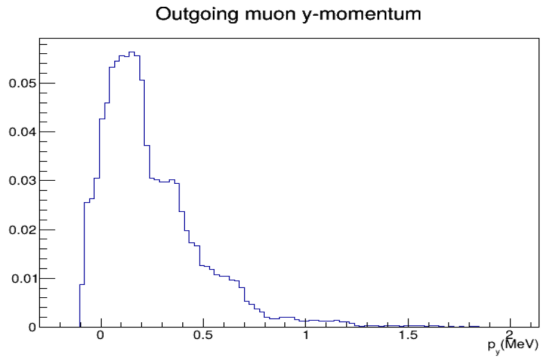

(b) p_y histogram for the outgoing muon

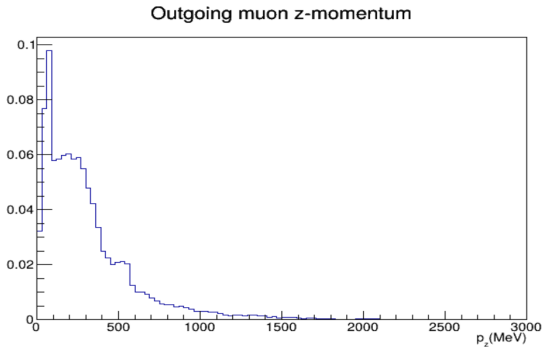

(c) p_z histogram for the outgoing muon

Figure A.1: muon momenta distributions for the outgoing muon of DH decays

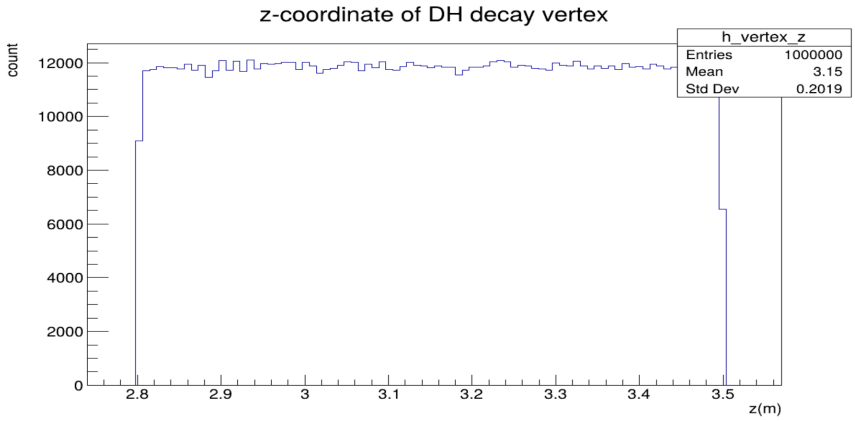

Figure A.2: z-coordinate distribution of the DH decay vertex